

## THE STABILITY OF MAGNETIZED ROTATING PLASMAS WITH SUPERTHERMAL FIELDS

MARTIN E. PESSAH<sup>1,2</sup> AND DIMITRIOS PSALTIS<sup>2,1</sup>*Draft version July 4, 2018*

## ABSTRACT

During the last decade it has become evident that the magnetorotational instability is at the heart of the enhanced angular momentum transport in weakly magnetized accretion disks around neutron stars and black holes. In this paper, we investigate the local linear stability of differentially rotating, magnetized flows and the evolution of the magnetorotational instability beyond the weak-field limit. We show that, when superthermal toroidal fields are considered, the effects of both compressibility and magnetic tension forces, which are related to the curvature of toroidal field lines, should be taken fully into account. We demonstrate that the presence of a strong toroidal component in the magnetic field plays a non-trivial role. When strong fields are considered, the strength of the toroidal magnetic field not only modifies the growth rates of the unstable modes but also determines which modes are subject to instabilities. We find that, for rotating configurations with Keplerian laws, the magnetorotational instability is stabilized at low wavenumbers for toroidal Alfvén speeds exceeding the geometric mean of the sound speed and the rotational speed. For a broad range of magnetic field strengths, we also find that two additional distinct instabilities are present; they both appear as the result of coupling between the modes that become the Alfvén and the slow modes in the limit of no rotation. We discuss the significance of our findings for the stability of cold, magnetically dominated, rotating fluids and argue that, for these systems, the curvature of toroidal field lines cannot be neglected even when short wavelength perturbations are considered. We also comment on the implications of our results for the validity of shearing box simulations in which superthermal toroidal fields are generated.

*Subject headings:* accretion, accretion disks — MHD — instabilities — plasmas

## 1. INTRODUCTION

Linear mode analyses provide a useful tool in gaining important insight into the relevant physical processes determining the stability of magnetized accretion flows. Studies of local linear modes of accretion disks threaded by weak magnetic fields have pointed out important clues on viable mechanisms for angular momentum transport and the subsequent accretion of matter onto the central objects (Balbus & Hawley 1991, 1998, 2002; Sano & Miyama 1999; Balbus 2003). They have also provided simplified physical models and analogies over which more complex physics can, in principle, be added (Balbus & Hawley 1992, 1998; Quataert, Dorland, & Hammett 2002). These treatments were carried out in the magnetohydrodynamic (MHD) limit (but see Quataert, Dorland & Hammett 2002 who studied the kinetic limit) and invoked a number of approximations appropriate to the study of the evolution of short-wavelength perturbations, when weak fields are considered. In this context, the strength of the magnetic field,  $B$ , is inferred by comparing the thermal pressure,  $P$ , to the magnetic pressure and is characterized by a plasma parameter,  $\beta \equiv 8\pi P/B^2 > 1$ .

It is not hard to find situations of astrophysical interest, however, in which the condition of weak magnetic fields is not satisfied. A common example of such a situation is the innermost region of an accretion disk around a magnetic neutron star. It is widely accepted that X-ray pulsars are powered by accretion of matter onto the polar caps of magnetic neutron stars. For this to occur, matter in the nearly Keplerian accretion disk has to be funneled along the field lines. This suggests that, at some radius, centrifugal forces and thermal pressure have to be overcome by magnetic stresses, leading naturally to regions where  $\beta \lesssim 1$ .

In the context of accretion disks, the presence of superthermal fields in rarefied coronae also seems hard to avoid, if coronal heating is a direct consequence of the internal dynamics of the disk itself rather than being produced by external irradiation from the central object. Three-dimensional MHD simulations by Miller & Stone (2000) showed that magnetic turbulence can effectively couple with buoyancy to transport the magnetic energy produced by the magnetorotational instability (MRI) in weakly magnetized disks to create a strongly magnetized corona within a few scale heights from the disk plane. On long time scales, the average vertical disk structure consists of a weakly magnetized ( $\beta \simeq 50$ ) turbulent core below two scale heights and a strongly magnetized ( $\beta \lesssim 0.1$ ) non-turbulent corona above it. The late stages of evolution in these models show that the disks themselves become magnetically dominated. Machida, Hayashi, & Matsumoto (2000) also found that the average plasma  $\beta$  in disk coronae is  $\simeq 0.1 - 1$  and the volume filling factor for regions with  $\beta \lesssim 0.3$  is up to 0.1. Even in the absence of an initial toroidal component, simulations carried out by Kudoh, Matsumoto, & Shibata (2002) showed that low- $\beta$  regions develop near the equator of the disk because of a strong toroidal component of the magnetic field generated by shear. On more theoretical grounds,

<sup>1</sup> Astronomy Department, University of Arizona, 933 N. Cherry Ave., Tucson, AZ, 85721; mpessah@as.arizona.edu

<sup>2</sup> Physics Department, University of Arizona, 1118 E. 4th St., Tucson, AZ, 85721; dpsaltis@physics.arizona.edu

strong toroidal magnetic fields produced by strong shear in the boundary layer region have been suggested as responsible for the observed bipolar outflows in young stellar objects (Pringle 1989). More recently, Pariev, Blackman, & Boldyrev (2003) found self-consistent solutions for thin magnetically-supported accretion disks and pointed out the necessity of assessing the stability properties of such configurations.

Another case in which magnetic fields seem to play an important dynamical role in rotating fluid configurations is that of magnetically supported molecular clouds. Observations of both large Zeeman line-splitting and of broad molecular lines support the presence of superthermal fields (see Myers & Goodman 1988 for further references and Bourke & Goodman 2003 for a review on the current understanding on the role of magnetic fields in molecular clouds). Values of the plasma  $\beta$  of the order of 0.1 – 0.01 have also been used in numerical studies of the structural properties of giant molecular clouds (Ostriker, Stone, & Gammie 2001).

As a last example of astrophysical interest, we mention magnetocentrifugally driven winds, such as those observed in protostars. These outflows seem to play an important role in the evolution of young stellar objects and in the dynamics of the parent clouds by providing a source of turbulent energy. Magnetocentrifugal jets typically involve internal Alfvén speeds comparable to the flow speeds. These structures are supported mainly by magnetic pressure due to strong toroidal fields. The ratio of magnetic pressure in the jet to the gas pressure of the ambient medium can be of the order of  $10^6$  (for an extensive study of MHD driven instabilities in these systems see Kim & Ostriker 2000 and §5.3).

In this paper, we investigate the local linear stability of differentially rotating flows without imposing any *a priori* restrictions on the strength of the magnetic field. We do, however, restrict our attention to rotationally supported flows (we loosely use this term to refer to flows with internal Alfvén speeds smaller than the rotational speed). Our intent is to demonstrate that the effects of the finite curvature of the toroidal field lines on the stability of small-wavelength vertical perturbations (i.e., on the most unstable modes present in the weak-field MRI) cannot be neglected when superthermal toroidal fields are present. In order to achieve this task, we relax the Boussinesq approximation (see also Papaloizou & Szuszkiewicz 1992 and Blaes & Balbus 1994), which is valid only when the toroidal component of the field is subthermal (Balbus & Hawley 1991). We thus consider the MHD fluid to be fully compressible. Moreover, even though we perform a local analysis, we do consider curvature terms when evaluating magnetic forces, for they become important in the strong-field regime (see also Knobloch 1992 and Kim & Ostriker 2000).

In most early studies addressing the MRI, it was found that the only role played by a toroidal component in the magnetic field is to quench the growth rates of the modes that are already unstable when only weak vertical fields are considered (Balbus & Hawley 1991; Blaes & Balbus 1994; see Quataert, Dorland, & Hammett 2002 for the kinetic limit; see also Kim & Ostriker 2000 for the cold MHD limit). Here, we show that, when strong fields are considered and the approximations usually invoked in the study of the weak-field MRI are relaxed, the presence of a toroidal component of the magnetic field plays a crucial role not only in the growth rates of the unstable modes but also in determining which modes are subject to instabilities<sup>3</sup>. As expected, the presence of a toroidal component breaks the symmetry of the problem, also giving rise to traveling modes. Moreover, for a broad range of magnetic field strengths, we find that two different instabilities are present. They both appear as the result of coupling between the modes that become the Alfvén and the slow mode in the limit of no rotation.

The paper is organized as follows. In §2, we describe the physical setup to be studied, present the dispersion relation to be solved, and discuss the importance of curvature terms in the limit of superthermal fields. In §3, we solve numerically the dispersion relation in some interesting regimes. In §4, we study the onset of instabilities as a function of magnetic field strengths and present some useful approximate criteria that enable us to study analytically some aspects of the full problem. In §5, we compare our results to previous investigations and discuss some of the implications of this study. Finally, in §6, we present a brief summary and our conclusions.

## 2. MHD EQUATIONS FOR PERTURBATIONS AND THE DISPERSION RELATION

We start with the set of equations that govern the behavior of a polytropic fluid in the MHD approximation,

$$\frac{\partial \rho}{\partial t} + \nabla \cdot (\rho \mathbf{v}) = 0, \quad (1)$$

$$\rho \frac{\partial \mathbf{v}}{\partial t} + (\rho \mathbf{v} \cdot \nabla) \mathbf{v} = -\rho \nabla \Phi - \nabla \left( P + \frac{\mathbf{B}^2}{8\pi} \right) + \left( \frac{\mathbf{B}}{4\pi} \cdot \nabla \right) \mathbf{B}, \quad (2)$$

$$\frac{\partial \mathbf{B}}{\partial t} + (\nabla \cdot \mathbf{v}) \mathbf{B} - (\mathbf{B} \cdot \nabla) \mathbf{v} + (\mathbf{v} \cdot \nabla) \mathbf{B} = 0, \quad (3)$$

and

$$P = P_0 \left( \frac{\rho}{\rho_0} \right)^\Gamma. \quad (4)$$

In these equations,  $\rho$  is the mass density,  $\mathbf{v}$  the velocity,  $P$  the gas pressure, and  $\Gamma$  the polytropic index;  $\mathbf{B}$  is the magnetic field and  $\Phi$  the gravitational potential. For convenience we adopt a cylindrical set of coordinates  $(r, \phi, z)$  with origin in the central object (i.e., the neutron star or black hole). We assume a steady axisymmetric background flow characterized by a velocity

<sup>3</sup> We will comment later in more detail on the paper by Curry & Pudritz (1995) who outlined the effects of a dynamically important toroidal field (in the case of an incompressible MHD flow) and address the similitudes and differences with our findings.

field of the form  $\mathbf{v} = v_\phi(r, z)\hat{\phi}$  and threaded by a background magnetic field. For consistency, our analysis is restricted to background fields of the form  $\mathbf{B} = B_\phi\hat{\phi} + B_z\hat{z}$  since the effect of including a radial component in the field is to generate a linear growth in time of the toroidal component (Balbus & Hawley 1991). Under these circumstances, all the background quantities depend on the radial and vertical coordinates only. In the present treatment, we neglect the self gravity of the fluid. In fact, Pariev, Blackman, & Boldyrev (2003) showed that magnetically dominated accretion disks have lower surface and volume densities for a fixed accretion rate. This suggests that these systems are lighter than standard disks and thus are not subject to self-gravity instabilities.

### 2.1. Equations for the Perturbations

In order to perform the local linear mode analysis, we perturb the set of equations (1)-(4) by substituting every physical variable  $f$  by  $f + \delta f$  and retain only linear orders in  $\delta f$ . In the following, we focus our analysis on the study of axisymmetric perturbations in an axisymmetric background.

We first consider, in some detail, the radial component of the momentum equation (2), which becomes

$$\begin{aligned} \frac{\partial \delta v_r}{\partial t} - 2\Omega \delta v_\phi + \frac{1}{\rho} \left[ \frac{\partial \delta P}{\partial r} + \frac{1}{4\pi} \left( \frac{\partial B_\phi}{\partial r} \delta B_\phi + B_\phi \frac{\partial \delta B_\phi}{\partial r} + \frac{\partial B_z}{\partial r} \delta B_z + B_z \frac{\partial \delta B_z}{\partial r} \right) \right] - \frac{\partial P}{\partial r} \frac{\delta \rho}{\rho^2} \\ - \frac{1}{4\pi \rho} \left( B_\phi \frac{\partial B_\phi}{\partial r} + B_z \frac{\partial B_z}{\partial r} \right) \frac{\delta \rho}{\rho} - \frac{1}{4\pi \rho} \left[ B_z \frac{\partial \delta B_r}{\partial z} - 2 \frac{B_\phi}{r} \delta B_\phi \right] - \frac{1}{4\pi \rho} \frac{B_\phi^2}{r} \frac{\delta \rho}{\rho} = 0. \end{aligned} \quad (5)$$

The coefficients in this linear equation for the perturbed variables depend in general on  $r$  and  $z$ , [e.g., the angular velocity  $\Omega$  is in general  $\Omega(r, z)$ ]. Therefore, at this point, the decomposition of perturbed quantities in Fourier modes – e.g., symbolically  $\delta f = \sum \delta f_k e^{i(k_r r + k_z z - \omega t)}$  – would not result in any particular simplification of the problem. This can be seen by taking the Fourier transform of equation (5) which results in a sum of convolutions of the Fourier transforms of background and perturbed quantities. Further progress can be made if we restrict the wavelengths of the perturbations for which our stability analysis is valid. To this end, we choose a fiducial point,  $\mathbf{r}_0 = (r_0, \phi_0, z_0)$ , around which we perform the local stability analysis. The choice of the particular value of  $\phi_0$  is, of course, irrelevant in the axisymmetric case under study.

We expand all the background quantities in equation (5) in Taylor series around  $\mathbf{r}_0$  and retain only the zeroth order in terms of the local coordinates  $\xi_r = r - r_0$  and  $\xi_z = z - z_0$  to obtain

$$\begin{aligned} \frac{\partial \delta v_r}{\partial t} - 2\Omega_0 \delta v_\phi + \frac{1}{\rho_0} \left[ \frac{\partial \delta P}{\partial \xi_r} + \frac{1}{4\pi} \left( \frac{\partial B_\phi}{\partial r} \Big|_0 \delta B_\phi + B_\phi^0 \frac{\partial \delta B_\phi}{\partial \xi_r} + \frac{\partial B_z}{\partial r} \Big|_0 \delta B_z + B_z^0 \frac{\partial \delta B_z}{\partial \xi_r} \right) \right] - \frac{\partial P}{\partial r} \Big|_0 \frac{\delta \rho}{\rho_0^2} \\ - \frac{1}{4\pi \rho_0} \left( B_\phi^0 \frac{\partial B_\phi}{\partial r} \Big|_0 + B_z^0 \frac{\partial B_z}{\partial r} \Big|_0 \right) \frac{\delta \rho}{\rho_0} - \frac{1}{4\pi \rho_0} \left( B_z^0 \frac{\partial \delta B_r}{\partial \xi_z} - 2 \frac{B_\phi^0}{r_0} \delta B_\phi \right) - \frac{1}{4\pi \rho_0} \frac{(B_\phi^0)^2}{r_0} \frac{\delta \rho}{\rho_0} = 0. \end{aligned} \quad (6)$$

Here,  $\Omega_0$ ,  $\rho_0$ ,  $B_\phi^0$ , and  $B_z^0$  stand for the angular velocity, background density, and magnetic field components at the fiducial point  $\mathbf{r}_0$  and the subscript “0” in the derivatives with respect to the radial coordinate  $r$  indicates that they are evaluated at  $\mathbf{r}_0$ . Equation (6) is a linear partial-differential equation in the local variables for the perturbed quantities but with constant coefficients. This is a good approximation as long as the departures  $(\xi_r, \xi_z)$  are small compared to the length scales over which there are significant variations in the background quantities, i.e.,  $\xi_r \ll L_r$  and  $\xi_z \ll L_z$ , where  $L_r$  and  $L_z$  are the characteristic length scales in the radial and vertical directions, respectively.

It is only now that it is useful to expand the perturbed quantities in equation (6) in Fourier modes. We can thus write each one of the perturbed quantities as

$$\delta f = \delta f(k_r, k_z, \omega) e^{i(k_r \xi_r + k_z \xi_z - \omega t)}, \quad (7)$$

and write the radial momentum equation for each mode as

$$\begin{aligned} -i\omega \delta v_r - 2\Omega_0 \delta v_\phi - ik_z \frac{B_z^0 \delta B_r}{4\pi \rho_0} + \left( ik_r + \frac{2}{r_0} + \frac{\partial \ln B_\phi}{\partial r} \Big|_0 \right) \frac{B_\phi^0 \delta B_\phi}{4\pi \rho_0} + \left( ik_r + \frac{\partial \ln B_z}{\partial r} \Big|_0 \right) \frac{B_z^0 \delta B_z}{4\pi \rho_0} \\ + \left\{ \left( ik_r - \frac{\partial \ln \rho}{\partial r} \Big|_0 \right) (c_s^0)^2 - \left[ \left( \frac{1}{r_0} + \frac{\partial \ln B_\phi}{\partial r} \Big|_0 \right) (v_{A\phi}^0)^2 + \frac{\partial \ln B_z}{\partial r} \Big|_0 (v_{Az}^0)^2 \right] \right\} \frac{\delta \rho}{\rho_0} = 0. \end{aligned} \quad (8)$$

Here, we have introduced the quantities  $c_s^0$ ,  $v_{A\phi}^0$  and  $v_{Az}^0$  that stand for the local sound speed and local Alfvén speeds associated with the toroidal and vertical components of the local magnetic field and are defined by

$$c_s^0 \equiv \sqrt{\Gamma \frac{P_0}{\rho_0}}, \quad v_{A\phi}^0 \equiv \frac{B_\phi^0}{\sqrt{4\pi \rho_0}}, \quad \text{and} \quad v_{Az}^0 \equiv \frac{B_z^0}{\sqrt{4\pi \rho_0}}. \quad (9)$$

Note that, for brevity, we have omitted the dependences  $(k_r, k_z, \omega)$  in the Fourier amplitudes. For consistency, the validity of the analysis is now restricted to modes with wavenumbers satisfying  $k_r L_r \gg 1$  and  $k_z L_z \gg 1$ . Without loss of generality,

we assume that the fiducial point is inside the disk so we can write the local conditions on the wavenumbers as  $k_r r_0 \gg 1$  and  $k_z z_0 \gg 1$ . Moreover, for fiducial points such that  $r_0 \geq z_0$  the latter condition also implies  $k_z r_0 \gg 1$ .

At this point, it is also convenient to define a new set of independent variables  $(\delta v_{Ar}, \delta v_{A\phi}, \delta v_{Az})$  defined in terms of  $(\delta B_r, \delta B_\phi, \delta B_z)$  in such a way that  $\delta \mathbf{v}_A \equiv \delta \mathbf{B} / \sqrt{4\pi\rho_0}$ . In this case, equation (8) reads

$$\begin{aligned} & -i\omega\delta v_r - 2\Omega_0\delta v_\phi - ik_z v_{Az}^0 \delta v_{Ar} + \left(ik_r + \frac{2}{r_0} + \frac{\partial \ln B_\phi}{\partial r}\bigg|_0\right) v_{A\phi}^0 \delta v_{A\phi} + \left(ik_r + \frac{\partial \ln B_z}{\partial r}\bigg|_0\right) v_{Az}^0 \delta v_{Az} \\ & + \left\{ \left(ik_r - \frac{\partial \ln \rho}{\partial r}\bigg|_0\right) (c_s^0)^2 - \left[ \left(\frac{1}{r_0} + \frac{\partial \ln B_\phi}{\partial r}\bigg|_0\right) (v_{A\phi}^0)^2 + \frac{\partial \ln B_z}{\partial r}\bigg|_0 (v_{Az}^0)^2 \right] \right\} \frac{\delta \rho}{\rho_0} = 0. \end{aligned} \quad (10)$$

As a last step, it is useful to work with dimensionless quantities. To this end, we define dimensionless variables by scaling all the frequencies with the local rotational frequency  $\Omega_0$  and all speeds with the local circular velocity  $\Omega_0 r_0$ . It is also convenient to define dimensionless wavenumbers by multiplying the physical wavenumber by the radial coordinate  $r_0$ . In summary, we define

$$\tilde{\omega} = \omega/\Omega_0, \quad \tilde{k}_r = k_r r_0, \quad \tilde{k}_z = k_z r_0, \quad (11)$$

$$\tilde{c}_s^0 = c_s^0/\Omega_0 r_0, \quad \tilde{v}_{A\phi}^0 = v_{A\phi}^0/\Omega_0 r_0, \quad \tilde{v}_{Az}^0 = v_{Az}^0/\Omega_0 r_0, \quad (12)$$

$$\delta \tilde{\rho} = \delta \rho/\rho_0, \quad \delta \tilde{\mathbf{v}} = \delta \mathbf{v}/\Omega_0 r_0, \quad \delta \tilde{\mathbf{v}}_A = \delta \mathbf{v}_A/\Omega_0 r_0. \quad (13)$$

For completeness, we introduce here the epicyclic frequency  $\kappa$  and its local dimensionless counterpart

$$\kappa = 2\Omega \left[ 1 + \frac{1}{2} \frac{d \ln \Omega}{d \ln r} \right]^{1/2} \quad \text{and} \quad \tilde{\kappa}_0 = \frac{\kappa_0}{\Omega_0} = 2 \left[ 1 + \frac{1}{2} \frac{d \ln \Omega}{d \ln r} \bigg|_0 \right]^{1/2}. \quad (14)$$

This quantity appears naturally in stability analyses of differentially rotating configurations and it is the frequency at which all the flow variables oscillate around their background values in the absence of magnetic fields. For a rotational profile given by a power law, the epicyclic frequency is proportional to the angular frequency at all radii.

Finally, the dimensionless version of equation (10) reads,

$$\begin{aligned} & -i\tilde{\omega}\delta \tilde{v}_r - 2\delta \tilde{v}_\phi - i\tilde{k}_z \tilde{v}_{Az}^0 \delta \tilde{v}_{Ar} + \left(i\tilde{k}_r + 2 + \frac{\partial \ln B_\phi}{\partial \ln r}\bigg|_0\right) \tilde{v}_{A\phi}^0 \delta \tilde{v}_{A\phi} + \left(i\tilde{k}_r + \frac{\partial \ln B_z}{\partial \ln r}\bigg|_0\right) \tilde{v}_{Az}^0 \delta \tilde{v}_{Az} \\ & + \left\{ \left(i\tilde{k}_r - \frac{\partial \ln \rho}{\partial \ln r}\bigg|_0\right) (\tilde{c}_s^0)^2 - \left[ \left(1 + \frac{\partial \ln B_\phi}{\partial \ln r}\bigg|_0\right) (\tilde{v}_{A\phi}^0)^2 + \frac{\partial \ln B_z}{\partial \ln r}\bigg|_0 (\tilde{v}_{Az}^0)^2 \right] \right\} \delta \tilde{\rho} = 0. \end{aligned} \quad (15)$$

Following a similar procedure with the remaining equations in the system (1)-(4), we arrive to the linear set of equations needed to perform the local stability analysis. For brevity, we now drop the hat in all the dimensionless variables and the superscript in  $\tilde{c}_s^0, \tilde{v}_{A\phi}^0$  and  $\tilde{v}_{Az}^0$ . We then write

$$-i\omega\delta\rho + \left(ik_r + \epsilon_4 + \frac{\partial \ln \rho}{\partial \ln r}\bigg|_0\right) \delta v_r + \left(ik_z + \frac{r_0}{z_0} \frac{\partial \ln \rho}{\partial \ln z}\bigg|_0\right) \delta v_z = 0, \quad (16)$$

$$\begin{aligned} & -i\omega\delta v_r - 2\delta v_\phi - ik_z v_{Az} \delta v_{Ar} + \left(ik_r + 2\epsilon_1 + \frac{\partial \ln B_\phi}{\partial \ln r}\bigg|_0\right) v_{A\phi} \delta v_{A\phi} + \left(ik_r + \frac{\partial \ln B_z}{\partial \ln r}\bigg|_0\right) v_{Az} \delta v_{Az} \\ & + \left\{ \left(ik_r - \frac{\partial \ln \rho}{\partial \ln r}\bigg|_0\right) c_s^2 - \left[ \left(\epsilon_2 + \frac{\partial \ln B_\phi}{\partial \ln r}\bigg|_0\right) v_{A\phi}^2 + \frac{\partial \ln B_z}{\partial \ln r}\bigg|_0 v_{Az}^2 \right] \right\} \delta \rho = 0, \end{aligned} \quad (17)$$

$$\begin{aligned} & -i\omega\delta v_\phi + \frac{\kappa^2}{2} \delta v_r + \frac{r_0}{z_0} \frac{\partial \ln \Omega}{\partial \ln z}\bigg|_0 \delta v_z - \left(\epsilon_3 + \frac{\partial \ln B_\phi}{\partial \ln r}\bigg|_0\right) v_{A\phi} \delta v_{Ar} \\ & - ik_z v_{Az} \delta v_{A\phi} - \frac{r_0}{z_0} \frac{\partial \ln B_\phi}{\partial \ln z}\bigg|_0 v_{A\phi} \delta v_{Az} = 0, \end{aligned} \quad (18)$$

$$\begin{aligned} & -i\omega\delta v_z - \frac{\partial \ln B_z}{\partial \ln r}\bigg|_0 v_{Az} \delta v_{Ar} + \left(ik_z + \frac{r_0}{z_0} \frac{\partial \ln B_\phi}{\partial \ln z}\bigg|_0\right) v_{A\phi} \delta v_{A\phi} \\ & + \left[ \left(ik_z - \frac{r_0}{z_0} \frac{\partial \ln \rho}{\partial \ln z}\bigg|_0\right) c_s^2 - \frac{r_0}{z_0} \left( \frac{\partial \ln B_\phi}{\partial \ln z}\bigg|_0 v_{A\phi}^2 + \frac{\partial \ln B_z}{\partial \ln z}\bigg|_0 v_{Az}^2 \right) \right] \delta \rho = 0, \end{aligned} \quad (19)$$

$$i\omega\delta v_{Ar} + ik_z v_{Az} \delta v_r = 0, \quad (20)$$

$$\begin{aligned}
& -i\omega\delta v_{A\phi} - \left. \frac{d\ln\Omega}{d\ln r} \right|_0 \delta v_{Ar} - \left. \frac{r_0}{z_0} \frac{d\ln\Omega}{d\ln z} \right|_0 \delta v_{Az} + \left( ik_r + \left. \frac{\partial \ln B_\phi}{\partial \ln r} \right|_0 \right) v_{A\phi} \delta v_r - ik_z v_{Az} \delta v_\phi \\
& + \left( ik_z + \left. \frac{r_0}{z_0} \frac{\partial \ln B_\phi}{\partial \ln z} \right|_0 \right) v_{A\phi} \delta v_z = 0,
\end{aligned} \tag{21}$$

and

$$-i\omega\delta v_{Az} + \left( ik_r + \epsilon_4 + \left. \frac{\partial \ln B_z}{\partial \ln r} \right|_0 \right) v_{Az} \delta v_r = 0, \tag{22}$$

where we have used equation (4) to recast the pressure perturbations in terms of density perturbations. The local conditions over the wavenumbers now read  $k_r \gg 1$  and  $k_z \gg 1$ .

The factors  $\epsilon_i$ , with  $i = 1, 2, 3, 4$ , are just convenient dummy variables that we introduce in order to help us keep track of the terms that account for the finite curvature of the background and are usually neglected in local studies of the weak-field MRI. Their numerical values are to be regarded as unity, unless otherwise mentioned. The terms proportional to  $\epsilon_1$  and  $\epsilon_2$  in equation (17) and the term proportional to  $\epsilon_3$  in equation (18) are due to the effects of magnetic tension and they appear naturally when a cylindrical coordinate system is adopted. The terms proportional to  $\epsilon_4$  in equations (16) and (22) are related to flux conservation in cylindrical coordinates. Although the three terms labeled by  $\epsilon_1$ ,  $\epsilon_2$ , and  $\epsilon_3$  share the same physical origin (i.e., magnetic tension introduced by the curvature of toroidal field lines), it is useful to be able to distinguish among them because the one labeled with  $\epsilon_2$  vanishes in the limit of an incompressible flow. Note that equations (20) and (22) ensure a divergence-free perturbed magnetic field, i.e.,  $\nabla \cdot \delta \mathbf{B} = 0$ , only when the finite curvature of the background is accounted for (i.e.,  $\epsilon_4 = 1$ ).

Up to this point, our intention has been to keep the discussion as general as possible in order to clearly state all the assumptions that we have made to obtain the set of equations for the perturbations to perform a local linear mode analysis. For the sake of simplicity, and to avoid the parametric study from being too extensive, we further invoke the following assumptions. We choose the fiducial point  $\mathbf{r}_0$  to lie in the disk mid-plane and assume that, locally, the vertical gradients in all background quantities are negligible and set them to zero. This will be a good approximation as long as we consider equilibrium configurations such that

$$\left| \frac{d\ln\rho}{d\ln z} \right|_0 \ll 1, \quad \left| \frac{d\ln B_\phi}{d\ln z} \right|_0 \ll 1, \quad \text{and} \quad \left| \frac{d\ln\Omega}{d\ln z} \right|_0 \ll 1. \tag{23}$$

Note that the solenoidal character of the magnetic field ensures that, for  $\mathbf{B} = B_\phi(r, z)\hat{\phi} + B_z(r, z)\hat{z}$ , the condition  $\partial B_z/\partial z = 0$  holds for arbitrary  $z$ .

In general, the forces induced by the curvature terms (e.g., the one proportional to  $\epsilon_2$  in eq. [17]) and those induced by background (logarithmic) gradients in the radial direction, (e.g., the term proportional to  $d\ln B_\phi/d\ln r|_0$  in the same equation) will not cancel each other. As a single exception, for the case in which  $B_\phi \propto r^{-1}$ , the most important effects due to the finite curvature of toroidal field lines are canceled out by the gradients in the toroidal field. This particular case, however, might not be completely relevant to realistic rotating flows since, in order to ensure force balance when the thermal pressure can be neglected against magnetic stresses, the magnetic field strength must decline more slowly than  $r^{-1}$  (see, e.g., Kim & Ostriker 2000). For simplicity, we further focus our attention on the study of differentially rotating, axisymmetric MHD flows with locally negligible radial gradients in the background density and magnetic field, i.e.,

$$\left| \frac{d\ln\rho}{d\ln r} \right|_0 \ll 1, \quad \left| \frac{d\ln B_\phi}{d\ln r} \right|_0 \ll 1, \quad \text{and} \quad \left| \frac{d\ln B_z}{d\ln r} \right|_0 \ll 1. \tag{24}$$

In the rest of the paper, we consider that the only background flow variable with a non-negligible local radial gradient is the angular velocity  $\Omega \propto r^{-q}$  and set all other radial gradients to zero. Note that this assumption is widely invoked in many investigations of the weak-field MRI (e.g., Blaes & Balbus 1994; Balbus & Hawley 1998; Blaes & Socrates 2001; Quataert, Dorland, & Hammett 2002; Balbus 2003). The assumption that the only background variable with a non-negligible radial gradient is the angular velocity is also generally a part of the initial set of conditions used in many numerical analyses of the MRI in the shearing box approximation (e.g., Hawley, Gammie, & Balbus 1994, 1995, 1996; Miller & Stone 2000).

In spite of being linear in the perturbed quantities, the terms proportional to  $\epsilon_i$  have been neglected in previous local studies of the MRI under the assumption that  $k_r \gg 1$  and  $k_z \gg 1$  (but see also Knobloch 1992 and Kim & Ostriker 2000). Although comparing an imaginary term against a real one in a stability analysis might seem particularly risky, this might not be a bad argument in order to neglect the terms proportional to  $\epsilon_1$  in equation (17) or  $\epsilon_4$  in equations (16) and (22) against  $ik_r$  (but see the discussion in Appendix A). The same could be said about the terms proportional to  $\epsilon_2$  in equation (17) or  $\epsilon_3$  in equation (18) in the limit of a very weak toroidal component in the magnetic field, given that both of them are proportional to  $v_{A\phi}$ . It is not evident, however, that we can neglect the terms proportional to either  $\epsilon_2$  in equation (17) or  $\epsilon_3$  in equation (18) if we are to explore the regime of strong toroidal fields. There are two different reasons for this. In order to neglect the term proportional to  $\epsilon_2$  against the one proportional to  $k_r$  in equation (17) we should be able to ensure that the condition  $(\epsilon_2/k_r)(v_{A\phi}^2/c_s^2) \ll 1$  is always satisfied, since both terms are proportional to  $\delta\rho$ . In this particular case, neglecting the forces induced by the bending of toroidal field lines becomes a progressively worse approximation the colder the disk is and is not well justified in the limit  $c_s \rightarrow 0$ . The case presented in equation (18) is even harder to justify a priori since now we would need to guarantee that the condition

$(\epsilon_3/k_z)(v_{A\phi}/v_{Az})(\delta v_{Ar}/\delta v_{A\phi}) \ll 1$  is always satisfied. However, this ratio is not only proportional to  $v_{A\phi}/v_{Az}$ , which might not be negligible in many astrophysical contexts but, through the ratio  $\delta v_{Ar}/\delta v_{A\phi}$ , is also a function of  $k_r$ ,  $k_z$ , and  $\omega(k_r, k_z)$ ; the magnitude of this term is therefore unknown until we solve the problem fully. A similar situation to this one is encountered if we aim to compare the term  $\epsilon_2 v_{A\phi}^2 \delta \rho$  with the term proportional to  $k_z v_{Az} \delta v_{Ar}$  in equation (17) (see §5.1 for further discussion).

For the sake of consistency and in order not to impose a constraint on the magnitude of the toroidal Alfvén speed with respect to the sound speed we keep all the terms proportional to the parameters  $\epsilon_i$ . We will later show that the term proportional to  $\epsilon_1$  is negligible when superthermal toroidal fields are considered. We will also discuss under which conditions the terms proportional to  $\epsilon_4$  can be neglected and why the terms proportional to  $\epsilon_2$  and  $\epsilon_3$  are particularly important.

## 2.2. Dispersion Relation

In order to seek for non-trivial solutions of the homogeneous system of linear equations (16)-(22) we set its determinant to zero. The resulting characteristic polynomial is

$$\begin{aligned} \omega^6 - \{ & (k_z^2 + k_r^2)(c_s^2 + v_{A\phi}^2 + v_{Az}^2) - ik_r[(2\epsilon_1 - \epsilon_2)v_{A\phi}^2 + \epsilon_4(c_s^2 + v_{Az}^2)] + k_z^2 v_{Az}^2 + \kappa^2 + \epsilon_2 \epsilon_4 v_{A\phi}^2 \} \omega^4 \\ & - (2\epsilon_1 + \epsilon_3) 2k_z v_{A\phi} v_{Az} \omega^3 + \left\{ k_z^2 v_{Az}^2 [(k_z^2 + k_r^2 - \epsilon_4 ik_r)(2c_s^2 + v_{A\phi}^2 + v_{Az}^2) + ik_r(\epsilon_2 - \epsilon_3)v_{A\phi}^2] \right. \\ & + k_z^2 \left[ \kappa^2(c_s^2 + v_{A\phi}^2) + 2\epsilon_1 \epsilon_4 c_s^2 v_{A\phi}^2 + \epsilon_2 \epsilon_4 v_{A\phi}^4 + 2 \frac{d \ln \Omega}{d \ln r} v_{Az}^2 + (\epsilon_2 \epsilon_4 - 2\epsilon_1 \epsilon_3) v_{A\phi}^2 v_{Az}^2 \right] \Big\} \omega^2 \\ & + 2k_z^3 v_{A\phi} v_{Az} [(2\epsilon_1 + \epsilon_3 + \epsilon_4)c_s^2 + (\epsilon_2 + \epsilon_3)v_{A\phi}^2] \omega \\ & - k_z^4 v_{Az}^2 \left[ (k_z^2 + k_r^2 - \epsilon_4 ik_r) c_s^2 v_{Az}^2 + 2 \frac{d \ln \Omega}{d \ln r} c_s^2 - 2\epsilon_1 \epsilon_3 c_s^2 v_{A\phi}^2 - \epsilon_2 \epsilon_3 v_{A\phi}^4 \right] = 0, \end{aligned} \quad (25)$$

where we have dropped the subscript “0” in the radial logarithmic derivative of the angular frequency. This is the most general dispersion relation under our current set of assumptions. When all the parameters  $\epsilon_i$  are set equal to zero, we recover the results of previous analyses where the curvature of the toroidal field lines was not considered (e.g., Blaes & Balbus 1994; Balbus & Hawley 1998), while when they are set equal to unity we obtain our full dispersion relation.

Although the original linear system (16)-(22) related seven variables (recall that we had eliminated  $\delta P$  in terms of  $\delta \rho$  using eq. [4] which is time-independent), the characteristic polynomial is only of 6<sup>th</sup> degree. This is easily understood by noting that equations (20) and (22) can be combined into one single equation expressing the solenoidal character of the perturbations in the magnetic field,  $\nabla \cdot \delta \mathbf{B} = 0$ . This implies a relationship between  $\delta B_r$  and  $\delta B_z$  (or equivalently between  $\delta v_{Ar}$  and  $\delta v_{Az}$ ) that must be satisfied at all times and is, therefore, independent of  $\omega$ . The fact that the dispersion relation (25) is of 6<sup>th</sup> and not of 4<sup>th</sup> degree is because we are taking into account the effects of finite compressibility. This can be seen immediately by taking the limit  $c_s \rightarrow \infty$ .

Once all the dimensionless variables have been properly defined, it is not evident that the magnetic-tension terms, proportional to  $\epsilon_1$ ,  $\epsilon_2$ , and  $\epsilon_3$ , will play a negligible role in determining the eigenfrequencies  $\omega$ . This is because the non-vanishing toroidal component of the magnetic field introduces odd powers in the dispersion relation and hence break its even symmetry. In fact, small modifications in the odd-power coefficients can and do have an important impact on the nature (real vs. complex) of the solutions. As we will see in §3 and describe in further detail in §4, these curvature terms introduce further coupling between the radial and toroidal directions, which in turn result in a strong coupling between the Alfvén and the slow mode.

Also important is the fact that some of the coefficients in the dispersion relation (25) are no longer real due to the factors  $ik_r$ . The presence of these terms does not allow us to affirm that complex roots will appear in conjugate pairs. As we discuss in Appendix A, the terms proportional to  $ik_r$  play an important role in determining the stability of modes for which the ratio  $k_r/k_z$  is non-negligible, even in the local limit, i.e., when  $k_r \gg 1$ . Of course the smaller the ratio  $k_r/k_z$ , the smaller the effects of the factors  $ik_r$  will be. If we consider the limit  $k_z \gg k_r$  in equation (25), the imaginary part of all the coefficients in the dispersion relation will become negligible. In this limiting case, whenever a given complex root is a solution of the dispersion relation (25) so is its complex conjugate, for the dispersion relation has real coefficients (see Appendix A).

In the next section, we will show that the dispersion relation (25) reduces to the dispersion relations previously derived in many local studies in different regimes. It is important to emphasize, however, that this dispersion relation fully considers the effects of compressibility and magnetic tension simultaneously without imposing any restrictions on the field strength or geometry. This feature is crucial in determining the stability properties of the MHD flow when strong toroidal fields are considered.

## 2.3. Previous Treatments

There has been some discussion in the past about the importance of the curvature terms for the stability of magnetized Keplerian flows (Knobloch 1992; Gammie & Balbus 1994). In studies in which these terms were considered (Knobloch 1992; Dubrulle & Knobloch 1993), compressibility effects were neglected. On the other hand, there have also been treatments in which compressibility was addressed but the curvature terms were neglected (Blaes & Balbus 1994). Both types of studies provided arguments for and against the importance of these terms. The limit of cold MHD flows has been addressed by Kim & Ostriker

(2000). These authors concluded that when the magnetic field strength is superthermal, the inclusion of toroidal fields tends to suppress the growth of the MRI and that for quasi-toroidal field configurations no axisymmetric MRI takes place in the limit  $c_s \rightarrow 0$ .

Because of the generality of our treatment, in which both curvature terms and compressibility effects are fully taken into account, we are able to address all of these issues in §5. For the time being, and as a check, we can take the appropriate limits in the general dispersion relation (25) to recover the dispersion relations derived in the aforementioned works.

*Compressibility with no field curvature* — Setting  $\epsilon_i = 0$ , for  $i = 1, 2, 3, 4$ , and considering perturbations propagating only in the vertical direction (this can be formally done by taking the limit  $k_z \gg k_r$  in equation [25]) we recover the dispersion relation derived in the compressible, weak-field limit by Blaes & Balbus (1994),

$$\begin{aligned} & \omega^6 - [k_z^2(c_s^2 + v_{A\phi}^2 + 2v_{Az}^2) + \kappa^2]\omega^4 \\ & + k_z^2 \left[ k_z^2 v_{Az}^2 (2c_s^2 + v_{A\phi}^2 + v_{Az}^2) + \kappa^2 (c_s^2 + v_{A\phi}^2) + 2 \frac{d \ln \Omega}{d \ln r} v_{Az}^2 \right] \omega^2 \\ & - k_z^4 v_{Az}^2 c_s^2 \left( k_z^2 v_{Az}^2 + 2 \frac{d \ln \Omega}{d \ln r} \right) = 0. \end{aligned} \quad (26)$$

The stability criterion derived from this dispersion relation is not different from the one derived, within the Boussinesq approximation, by Balbus & Hawley (1991). All the perturbations with vertical wavenumber smaller than the critical wavenumber  $k_{BH}$  are unstable, with

$$k_{BH}^2 v_{Az}^2 \equiv -2 \frac{d \ln \Omega}{d \ln r}. \quad (27)$$

In this case, the strength of the toroidal component of the magnetic field does not play any role in deciding which modes are subject to instabilities.

*Field curvature with no compressibility* — It is important to stress that even in the incompressible limit not all the terms proportional to  $\epsilon_i$  in the dispersion relation (25) are negligible (of course, the ones proportional to  $\epsilon_2$  are). To see that this is the case, we can take the limit  $c_s \rightarrow \infty$  in the dispersion relation (25) to obtain

$$\begin{aligned} & (k_z^2 + k_r^2 - ik_r \epsilon_4) \omega^4 - k_z^2 [2v_{Az}^2 (k_z^2 + k_r^2 - \epsilon_4 ik_r) + \kappa^2 + 2\epsilon_1 \epsilon_4 v_{A\phi}^2] \omega^2 - 2k_z^3 v_{A\phi} v_{Az} (2\epsilon_1 + \epsilon_3 + \epsilon_4) \omega \\ & + k_z^4 v_{Az}^2 \left[ (k_z^2 + k_r^2 - \epsilon_4 ik_r) v_{Az}^2 + 2 \frac{d \ln \Omega}{d \ln r} - 2\epsilon_1 \epsilon_3 v_{A\phi}^2 \right] = 0, \end{aligned} \quad (28)$$

where we have explicitly left the factors  $\epsilon_i$  that should be considered as unity. This incompressible version of our dispersion relation is to be compared with the one obtained by Dubrulle & Knobloch (1993) as the local limit of the corresponding eigenvalue problem. Note that, in order to compare expression (28) with the dispersion relation (eq. [37]) presented in Dubrulle & Knobloch (1993), it is necessary to consider the limit  $\partial v_{A\phi}/\partial r, \partial v_{Az}/\partial r \rightarrow 0$  in their equation (9). We also note that the radial wavenumber  $k_r$  appears in equation (28) only in the combination  $k_z^2 + k_r^2 - ik_r$  while in equation (37) in Dubrulle & Knobloch (1993) we only find it as  $k_z^2 + k_r^2$  (i.e.,  $n^2 + k^2$  in their notation). This is because when taking the local limit,  $k_r \gg 1$ , in the process of deriving their equation (37) from their equation (9), the terms proportional to  $ik_r$  were neglected against  $k_r^2$  by Dubrulle & Knobloch (1993).

When the toroidal component of the magnetic field is negligible, i.e., when  $v_{A\phi} \rightarrow 0$  in equation (28), and we consider vertical modes ( $k_z \gg k_r$ ), we recover the dispersion relation for the incompressible MRI; the onset of unstable modes is still given by expression (27). For weak toroidal fields, i.e., when  $v_{A\phi} \ll 1$ , we can read off the small corrections to the critical wavenumber from the constant coefficient,

$$(k_z^{0i})^2 v_{Az}^2 = -2 \frac{d \ln \Omega}{d \ln r} + 2\epsilon_1 \epsilon_2 v_{A\phi}^2. \quad (29)$$

For stronger fields, however, the  $\omega = 0$  mode is no longer unstable (see the Appendix B for a general discussion on the stability of the  $\omega = 0$  mode when compressibility and curvature terms are considered) and it is necessary to solve equation (28) in order to find the critical wavenumber for the onset of the instability. Roughly speaking, we would expect the solutions of equation (28) to depart significantly from the solutions to the incompressible version of the dispersion relation (26) when  $v_{A\phi}^2 \gtrsim |d \ln \Omega / d \ln r|$ , or  $v_{A\phi} \gtrsim 1.2$  for a Keplerian disk. Since in this paper we consider rotationally supported configurations (i.e.,  $v_{A\phi} \lesssim 1$ ), we will not address the modifications to the mode structure caused by curvature terms in incompressible MHD flows.

It is important to stress that, for both dispersion relations (26) and (28), in the case of rotationally supported disks, the stability criterion is insensitive (or, at most, very weakly sensitive, in the incompressible case) to the magnitude of the toroidal component of the field. As we will see throughout our study, the stability criteria that emerge from equation (25) are significantly different from the ones discussed in this section, when we consider fields for which  $v_{A\phi} > c_s$ . We will also see that the term proportional to  $\epsilon_2$ , which depends on curvature and compressibility effects and is, therefore, absent from either equation (26) or (28), plays an important role in determining the mode structure in the general case.

*Cold limit with no field curvature* — Another limit of interest is the one corresponding to the cold, MHD, cylindrical shearing flows usually involved in the modeling of cold disk winds (i.e., far away from the disk). In this context, Kim & Ostriker (2000)

addressed the behavior of the compressible axisymmetric MRI in the limit  $c_s \rightarrow 0$ . These authors obtained a dispersion relation considering both vertical and radial wavenumbers and derived the criterion for instability associated with it. Their dispersion relation in the fully compressible case [eq. (57)] reads

$$\begin{aligned} & \omega^6 - [(k_z^2 + k_r^2)(c_s^2 + v_{A\phi}^2 + v_{Az}^2) + k_z^2 v_{Az}^2 + \kappa^2] \omega^4 \\ & + k_z^2 \left[ (k_z^2 + k_r^2) v_{Az}^2 (2c_s^2 + v_{A\phi}^2 + v_{Az}^2) + \kappa^2 (c_s^2 + v_{A\phi}^2) + 2 \frac{d \ln \Omega}{d \ln r} v_{Az}^2 \right] \omega^2 \\ & - k_z^4 v_{Az}^2 c_s^2 \left[ (k_z^2 + k_r^2) v_{Az}^2 + 2 \frac{d \ln \Omega}{d \ln r} \right] = 0. \end{aligned} \quad (30)$$

This dispersion relation can be obtained from equation (25) if we set  $\epsilon_i = 0$ , for  $i = 1, 2, 3, 4$ . Note that if we take the limit  $k_z \gg k_r$  in equation (30) we recover equation (26).

For extremely cold flows we can take the limit  $c_s \rightarrow 0$  in equation (30) to obtain

$$\omega^4 - [(k_z^2 + k_r^2)(v_{A\phi}^2 + v_{Az}^2) + k_z^2 v_{Az}^2 + \kappa^2] \omega^2 + k_z^2 v_{Az}^2 (k_z^2 + k_r^2)(v_{A\phi}^2 + v_{Az}^2) + \kappa^2 k_z^2 v_{A\phi}^2 + 2 k_z^2 v_{Az}^2 \frac{d \ln \Omega}{d \ln r} = 0. \quad (31)$$

On the other hand, taking the limit  $c_s \rightarrow 0$  in equation (25), we obtain the more general dispersion relation

$$\begin{aligned} & \omega^6 - \{ (k_z^2 + k_r^2)(v_{A\phi}^2 + v_{Az}^2) - i k_r [(2\epsilon_1 - \epsilon_2) v_{A\phi}^2 + \epsilon_4 v_{Az}^2] + k_z^2 v_{Az}^2 + \kappa^2 + \epsilon_2 \epsilon_4 v_{A\phi}^2 \} \omega^4 \\ & - (2\epsilon_1 + \epsilon_3) 2 k_z v_{A\phi} v_{Az} \omega^3 + \left\{ k_z^2 v_{Az}^2 [(k_z^2 + k_r^2 - \epsilon_4 i k_r)(v_{A\phi}^2 + v_{Az}^2) + i k_r (\epsilon_2 - \epsilon_3) v_{A\phi}^2] \right. \\ & + k_z^2 \left[ \kappa^2 v_{A\phi}^2 + \epsilon_2 \epsilon_4 v_{A\phi}^4 + 2 \frac{d \ln \Omega}{d \ln r} v_{Az}^2 + (\epsilon_2 \epsilon_4 - 2\epsilon_1 \epsilon_3) v_{A\phi}^2 v_{Az}^2 \right] \} \omega^2 \\ & + 2 k_z^3 v_{A\phi} v_{Az} (\epsilon_2 + \epsilon_3) v_{A\phi}^2 \omega + k_z^4 v_{Az}^2 \epsilon_2 \epsilon_3 v_{A\phi}^4 = 0. \end{aligned} \quad (32)$$

Note that in this expression, as it was also the case in the incompressible limit, several of the terms that are due to the finite curvature of the toroidal field lines are still present.

Analyzing the limit  $c_s \rightarrow 0$  in the dispersion relation (30), Kim & Ostriker (2000) concluded that toroidal fields tend to suppress the growth of the MRI and that, for a Keplerian rotation law, no axisymmetric MRI occurs if  $i < 30^\circ$ , where  $i$  is the local pitch angle of the magnetic fields defined by  $i \equiv \tan^{-1}(v_{Az}/v_{A\phi})$ . However, the eigenfrequencies satisfying the dispersion relations (25) and (30) in the limit  $c_s \rightarrow 0$  are different and so are the criteria for instability which they are subject to. In §5.3, we comment in more detail on how the solutions to the dispersion relations (25) and (30) differ in the limit  $c_s \rightarrow 0$  and on the implications regarding the stabilization of the MRI in cold MHD shearing flows.

In order to investigate how previous results from local stability analyses of the weak field MRI are modified as the strength of the toroidal field component increases, we will focus our attention on the stability of modes with  $k_z \gg k_r$ .<sup>4</sup> This approach is physically motivated, since vertical modes correspond to the most unstable modes in the well studied MRI, and is also more tractable mathematically. In the next two sections, we will perform a thorough numerical and semi-analytical study of the general dispersion relation (25) in the limit  $k_z \gg k_r$ , with particular emphasis on the case of strong toroidal fields. We will then be in a better position to understand the similitudes and differences of our findings with those of the aforementioned studies and we will address them in §5.

### 3. NUMERICAL SOLUTIONS

We solved numerically the dispersion relation (25) for the frequency  $\omega$  as a function of the wavenumber  $k_z$ , employing Laguerre's root finding method (Press et al. 1992). As a typical situation of interest, we consider a Keplerian disk with  $c_s = 0.05$  and  $v_{Az} = 0.01$ . As it will be seen from the range of values of  $k_z$  in which the various instabilities occur, the case of quasi-toroidal superthermal fields is perfectly suited to be studied in the local approximation, i.e., when  $k_z \gg 1$ , provided that the vertical component of the magnetic field is weak enough (i.e.,  $v_{Az} \ll 1$ ).

To better appreciate the effects that the curvature terms have on the stability of the modes, a set of solutions to the dispersion relation (25) is shown in Figures 1 and 2.<sup>5</sup> Each of the three panels, in both figures, shows the real and imaginary parts of the solutions for different values of the toroidal field strength, parameterized by  $v_{A\phi}$ . The left panel shows the solutions to the full dispersion relation (25), i.e., when  $\epsilon_1 = \epsilon_2 = \epsilon_3 = \epsilon_4 = 1$ . The central panel shows the solutions to equation (25) when compressibility is neglected in the curvature terms, i.e., when  $\epsilon_1 = \epsilon_3 = \epsilon_4 = 1$  and  $\epsilon_2 = 0$ . For the sake of comparison, the right panel shows the solutions to the dispersion relation (26), in which all curvature terms are neglected.

We first analyze Figure 1. When all magnetic tension terms are neglected (right panel), the qualitative structure of the normal modes of the plasma is insensitive to the magnitude of the toroidal field component (see Blaes & Balbus 1994). However, the

<sup>4</sup> In Appendix A, we briefly describe how this results are modified when finite ratios  $k_r/k_z$  are considered.

<sup>5</sup> Some animations of the results presented in Figs. 1, 2, 7, and 8 are available at <http://www.physics.arizona.edu/~mpessah/research/>



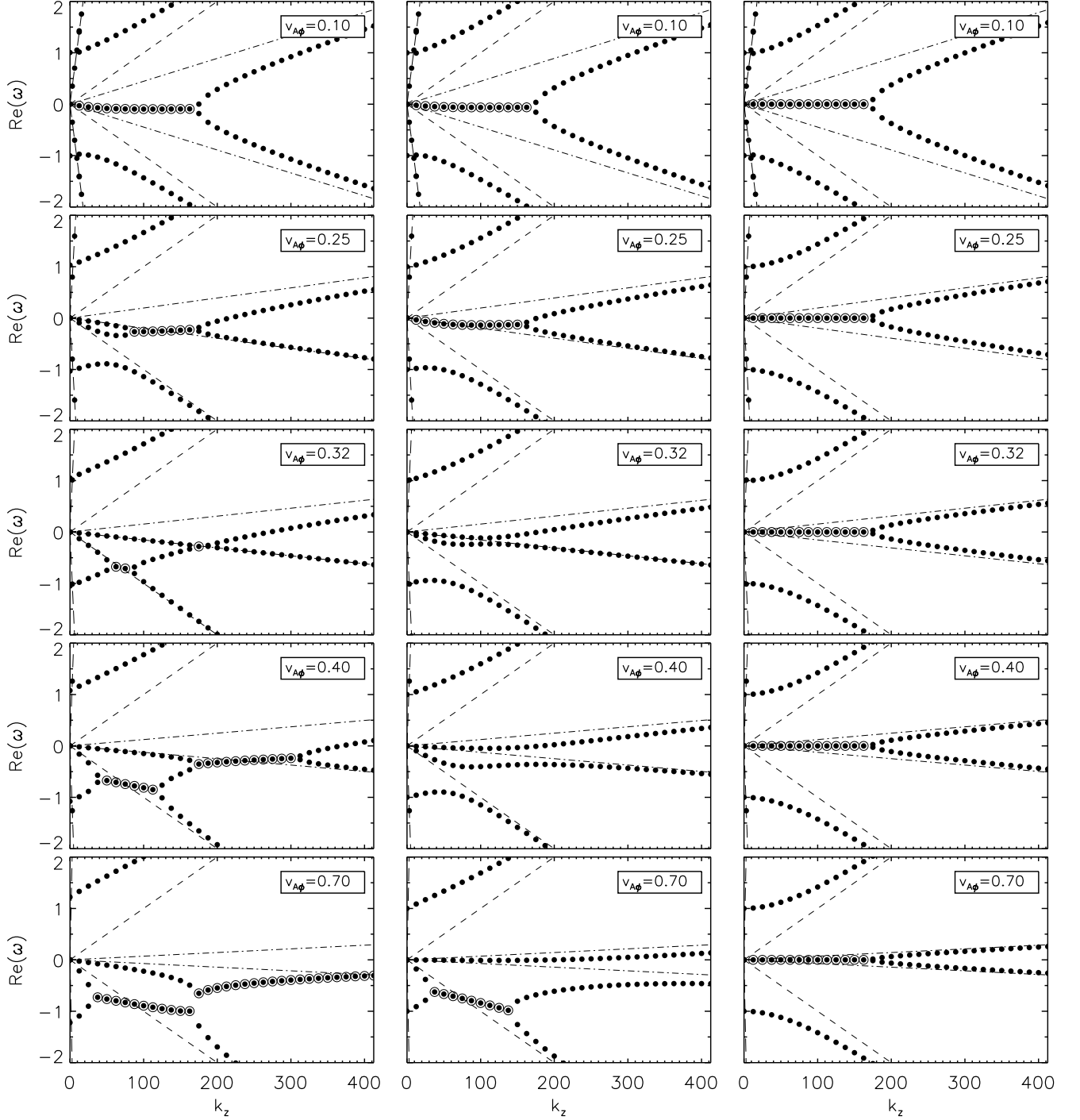


FIG. 1.— The real parts of the numerical solutions to the dispersion relation (25) corresponding to a Keplerian disk with  $c_s = 0.05$  and  $v_{Az} = 0.01$ . *Left panel:* solutions to the full problem ( $\epsilon_1 = \epsilon_2 = \epsilon_3 = \epsilon_4 = 1$ ). *Central panel:* the case in which compressibility is neglected in the curvature terms ( $\epsilon_1 = \epsilon_3 = \epsilon_4 = 1$  and  $\epsilon_2 = 0$ ). *Right panel:* the case in which all curvature terms are neglected ( $\epsilon_1 = \epsilon_2 = \epsilon_3 = \epsilon_4 = 0$ ). Open circles indicate unstable modes (i.e., those with positive imaginary part). Long-dashed, short-dashed, and point-dashed lines show the fast, Alfvén, and slow modes, respectively, in the limit of no rotation.

situation is very different when the magnetic tension terms are included. For weak toroidal fields, i.e., when  $v_{A\phi} \lesssim 0.1$ , the solutions seem quite insensitive to the curvature terms; indeed these terms do not seem to play a significant role in altering the local stability properties of magnetized Keplerian flows compared to what is quoted elsewhere in the literature. As we will see later, for a Keplerian disk, the presence of the curvature terms is significant once  $v_{A\phi}^2 \gtrsim c_s$ , which in this case translates into  $v_{A\phi} \gtrsim 0.22$ .

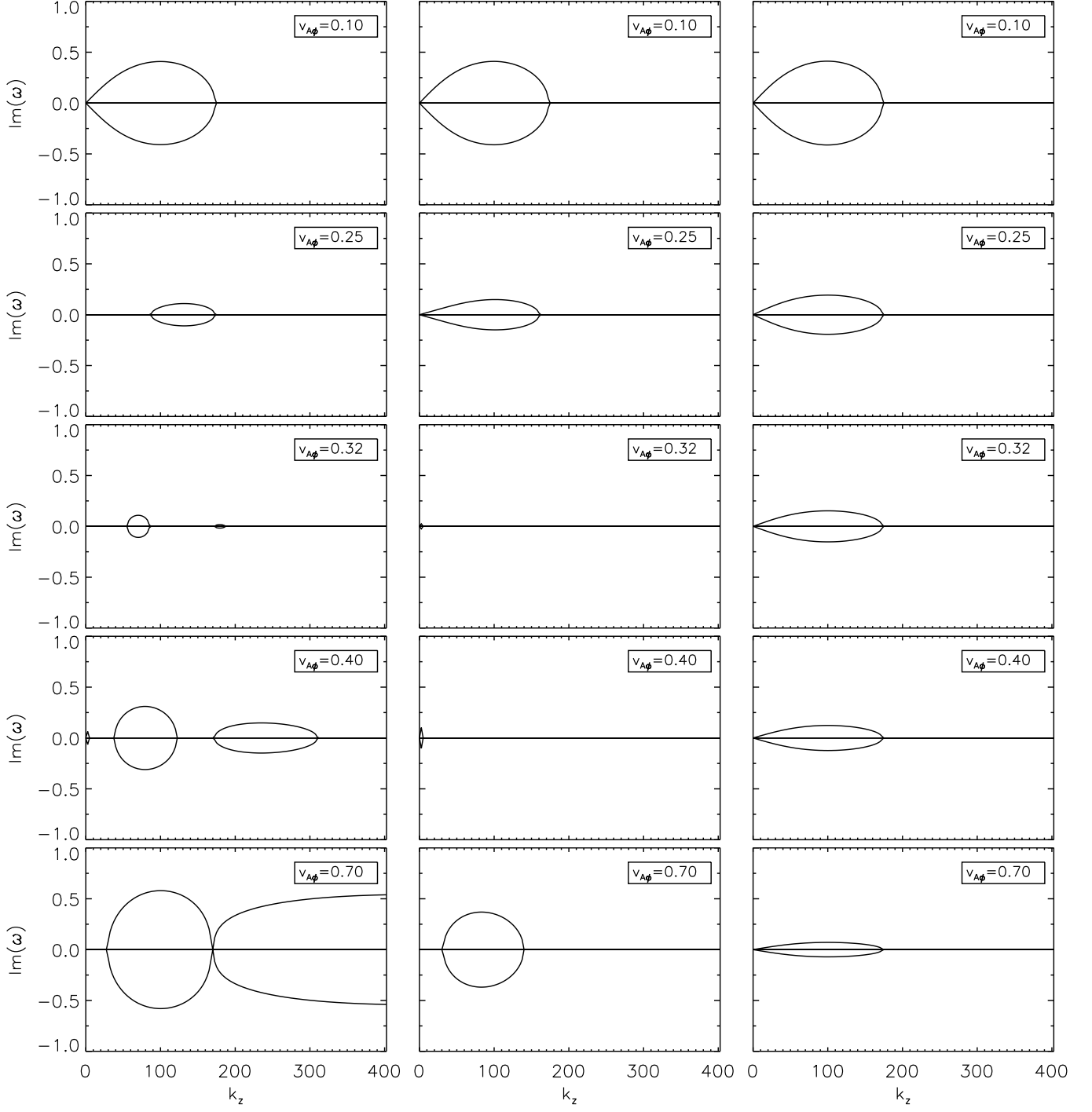


FIG. 2.— The imaginary parts for the cases discussed in Figure 1.

For stronger toroidal fields, i.e., when  $v_{A\phi} \gtrsim 0.2$ , the modes with the longest wavelengths become stable when all curvature terms are included, in sharp contrast to the case in which  $\epsilon_2 = 0$ . For even stronger toroidal fields, i.e., when  $v_{A\phi} \gtrsim 0.3$ , a second instability appears at long wavelengths, while the original instability is suppressed. When  $v_{A\phi} \gtrsim 0.4$ , both instabilities coexist as separate entities and the original instability reaches smaller and smaller spatial scales, when the magnitude of the toroidal field increases. For even higher toroidal fields, i.e., when  $v_{A\phi} \gtrsim 0.7$ , the largest unstable wavenumber of the instability that developed for  $v_{A\phi} \gtrsim 0.3$  approaches  $k_{\text{BH}}$  (see eq. [27]). The major implication of neglecting compressibility in the curvature terms is that the original instability seems to be totally suppressed for toroidal fields larger than the ones corresponding to  $v_{A\phi} \gtrsim 0.3$ .

As it is clear from the dispersion relation (25), the presence of the toroidal component in the field introduces odd powers of the mode frequency  $\omega$  and hence breaks the symmetry between positive and negative real parts of the solutions. The physical meaning of this is clear. The phase velocities of the instabilities are no longer zero and they are propagating vertically throughout the disk. This, of course, is not the case for the unstable solutions to the dispersion relation (26) regardless of the magnitude of  $v_{A\phi}$ . In that case, the most noticeable effect of an increasing toroidal field is to reduce the phase velocity of the stable modes beyond  $k_{BH}$  (which is itself independent of  $v_{A\phi}$ ).

It is also interesting to analyze how the presence of the curvature terms modifies the growth rates of the unstable modes as a function of the toroidal magnetic field. This is shown in Figure 2. Again, there are no significant changes for  $v_{A\phi} \lesssim 0.1$ ; however, quite significant modifications to the growth rates are present for  $v_{A\phi} \gtrsim 0.2$ . The sequence of plots in the left panel shows more clearly the suppression of the original instability, the appearance of the instability at low wavenumbers, the return of the instability at high wavenumbers, and finally the fusion of these last two. The right panel in this figure shows the effects that the presence of a strong toroidal component has on the mode structure when curvature terms are not considered. In this case, the critical wavenumber for the onset of instabilities is not modified while there is a clear reduction in the growth rate of the non-propagating unstable modes as the magnitude of the toroidal field component increases. When the curvature terms are considered fully, the effects are more dramatic. Note also that the growth rate of the original instability is reduced faster from the first to the second plot in the left panel in Figure 2 with respect to their counterparts in the right panel of the same figure.

#### 4. THE ONSET OF INSTABILITIES

##### 4.1. Unstable Modes

In §3 we presented how the structure of the various modes evolves as a function of the toroidal field strength and noted that, for a range of field strengths, two different instabilities are clearly distinguishable. Here, we obtain the conditions (i.e., the range of wavenumbers and toroidal field strengths) for which these unstable modes are present. We start by plotting in Figure 3 the range of unstable wavenumbers as a function of the toroidal field strength. As a reference, we have plotted the case for a Keplerian disk. The black dots in the diagram represent the unstable vertical wavenumbers, in units of  $k_z v_{Az}/c_s$ , for a given toroidal Alfvén speed, in terms of  $v_{A\phi}/c_s$ . Three regions of unstable modes are clearly distinguishable:

- *Region I* shows the evolution of the original instability present in the topmost three plots in the left panel in Figure 1. This is the region where the MRI lives. Strictly speaking, the MRI is confined to the region where  $v_{A\phi}/c_s \ll 1$ . As we will comment in §4.2, instability I is no longer incompressible beyond this point. The maximum wavenumber for which this instability exists is independent of  $v_{A\phi}$  and corresponds to the critical wavenumber for the onset of the MRI (i.e.,  $k_{BH}$  in eq. [27]). The stabilization of the long-wavelength perturbations beyond a critical value of the toroidal Alfvén speed is also evident in this region. For larger toroidal field strengths, shorter and shorter wavelengths are stabilized up to the ones corresponding to  $k_{BH}$ .
- *Region II* represents the evolution of the instability that is only present for wavenumbers  $k_z > k_{BH}$ . Note that  $k_{BH}$  is now the minimum wavenumber for the onset of instability II. In this case, increasing  $v_{A\phi}/c_s$  gives rise to unstable modes with even shorter wavelengths (two bottommost plots in the left panel of either Figure 1 or 2).
- *Region III* shows the instability that appears for intermediate wavenumbers (see for example the third plot in the left panel in Figure 1). Note that the shortest unstable wavelength in this region approaches  $k_{BH}$  for large values of  $v_{A\phi}/c_s$  (i.e., bottommost plot in the left panel of either Figure 1 or 2).

##### 4.2. Analytic Approximations

In this section we obtain analytical approximations to the dispersion relation (25) in various limits, which will help us identify the different critical curves in Figure 3.

The fast (or magnetosonic) modes are reasonably well decoupled from the rest of the oscillations (see left panels in Fig.1). By studying the modes that satisfy the condition  $\omega^2 \ll k_z^2 c_s^2$ , we effectively eliminate the fast modes from our analysis. This can be done for strong toroidal fields because, even in the presence of rotation, the magnetosonic modes are well described by  $\omega^2 \simeq k_z^2 (c_s^2 + v_A^2)$ . Note that imposing  $\omega^2 \ll k_z^2 c_s^2$  is a distinct and weaker condition than asking for the MHD fluid to be incompressible ( $c_s \rightarrow \infty$ ). By eliminating these fastest modes, it is possible to find a 4<sup>th</sup> degree dispersion relation in  $\omega$ , with solutions that constitute a very good approximation to the interesting modes seen in Figures 1 and 2.

We first write the equations for the evolution of the perturbations in the magnetic field. For the sake of clarity, we present the intermediate steps with the appropriate physical dimensions but we drop the index indicating local values. Substituting equations (16), (20), and (22) in equation (19) we obtain  $\delta v_z$  in terms of  $\delta B_\phi$  and  $\delta B_z$ ,

$$\delta v_z = -\frac{k_z \omega c_s^2}{(k_z c_s)^2 - \omega^2} \left[ \frac{v_{A\phi}^2}{c_s^2} \frac{\delta B_\phi}{B_\phi} + \frac{\delta B_z}{B_z} \right]. \quad (33)$$

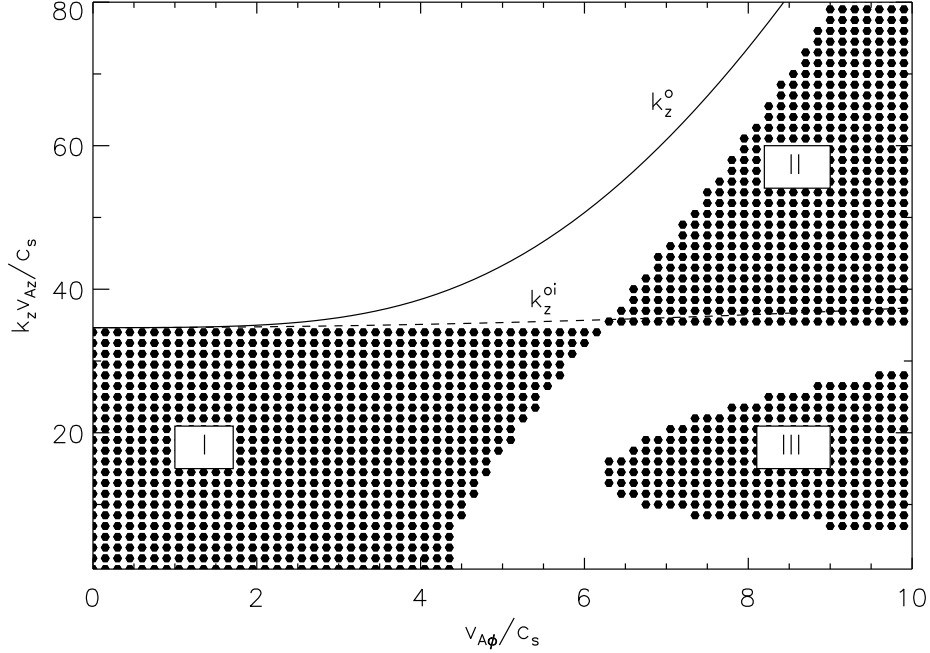


FIG. 3.— The black dots represent unstable modes obtained from solving the dispersion relation (25) numerically for a Keplerian disk with  $c_s = 0.05$  and  $v_{A\phi} = 0.01$ . The solid ( $k_z^o$ ) and dashed ( $k_z^{oi}$ ) lines correspond to the critical wavenumber for which the  $\omega = 0$  mode exists in the case of a compressible (see Appendix B) and an incompressible (discussed in §2) flow, respectively. For strong toroidal fields, compressibility plays a crucial role in the stability of the  $\omega = 0$  mode. Note that, in the limit of small  $v_{A\phi}/c_s$  we have  $k_z^o, k_z^{oi} \rightarrow k_{\text{BH}}$ , and the trivial mode becomes unstable.

Using this result in equation (21) we find,

$$ik_z B_z \delta v_\phi = -\frac{d\Omega}{d \ln r} \delta B_r - i\omega \delta B_\phi - i\omega B_\phi \frac{(k_z c_s)^2}{(k_z c_s)^2 - \omega^2} \left[ \frac{v_{A\phi}^2}{c_s^2} \frac{\delta B_\phi}{B_\phi} + \frac{\delta B_z}{B_z} \right]. \quad (34)$$

From equations (16), (22), and (33) we can recast  $\delta \rho$  in terms of  $\delta B_\phi$  and  $\delta B_z$  as

$$\frac{\delta \rho}{\rho} = -\frac{k_z^2 v_{A\phi}^2}{(k_z c_s)^2 - \omega^2} \frac{\delta B_\phi}{B_\phi} + \left[ 1 - \frac{(k_z c_s)^2}{(k_z c_s)^2 - \omega^2} \right] \frac{\delta B_z}{B_z}. \quad (35)$$

Finally, we can write equations (33)-(35) for the modes with frequencies such that  $\omega^2 \ll k_z^2 c_s^2$  as,

$$\delta v_z = -\frac{\omega}{k_z} \left[ \left( \frac{v_{A\phi}}{c_s} \right)^2 \frac{\delta B_\phi}{B_\phi} + i \frac{\epsilon_4}{k_z r} \frac{\delta B_r}{B_z} \right], \quad (36)$$

$$ik_z B_z \delta v_\phi = -\left[ \frac{d\Omega}{d \ln r} - \frac{\epsilon_4}{r} \frac{\omega}{k_z} \frac{B_\phi}{B_z} \right] \delta B_r - \left[ 1 + \left( \frac{v_{A\phi}}{c_s} \right)^2 \right] i\omega \delta B_\phi, \quad (37)$$

and

$$\frac{\delta \rho}{\rho} = -\frac{v_{A\phi}^2}{c_s^2} \frac{\delta B_\phi}{B_\phi}, \quad (38)$$

where we have used equations (20) and (22) to recast  $\delta B_z$  in terms of  $\delta B_r$ . Note that, neglecting the factor  $\omega^2$  against  $k_z^2 c_s^2$  in equation (33), and therefore in equations (34) and (35), effectively reduces to neglecting the term proportional to  $\omega$  in equation (19). Thus, for the modes of interest, the condition  $\omega^2 \ll k_z^2 c_s^2$  is a statement about force balance in the vertical direction, which is made explicit in equation (38). In this way, we can see how important perturbations in the density are, in the presence of strong toroidal fields (see also Balbus & Hawley 1991). For  $v_{A\phi} \gg c_s$ , even small variation in the toroidal component of the field can have an important impact on the dynamics of the perturbations. For this reason, the assumption of an incompressible MHD flow is not valid, whenever superthermal toroidal fields are considered. Note that, in order to recover the incompressible MRI when  $\epsilon_i = 0$ , for  $i = 1, 2, 3, 4$ , we have not neglected the factor unity against  $(v_{A\phi}/c_s)^2$ , in equation (37).

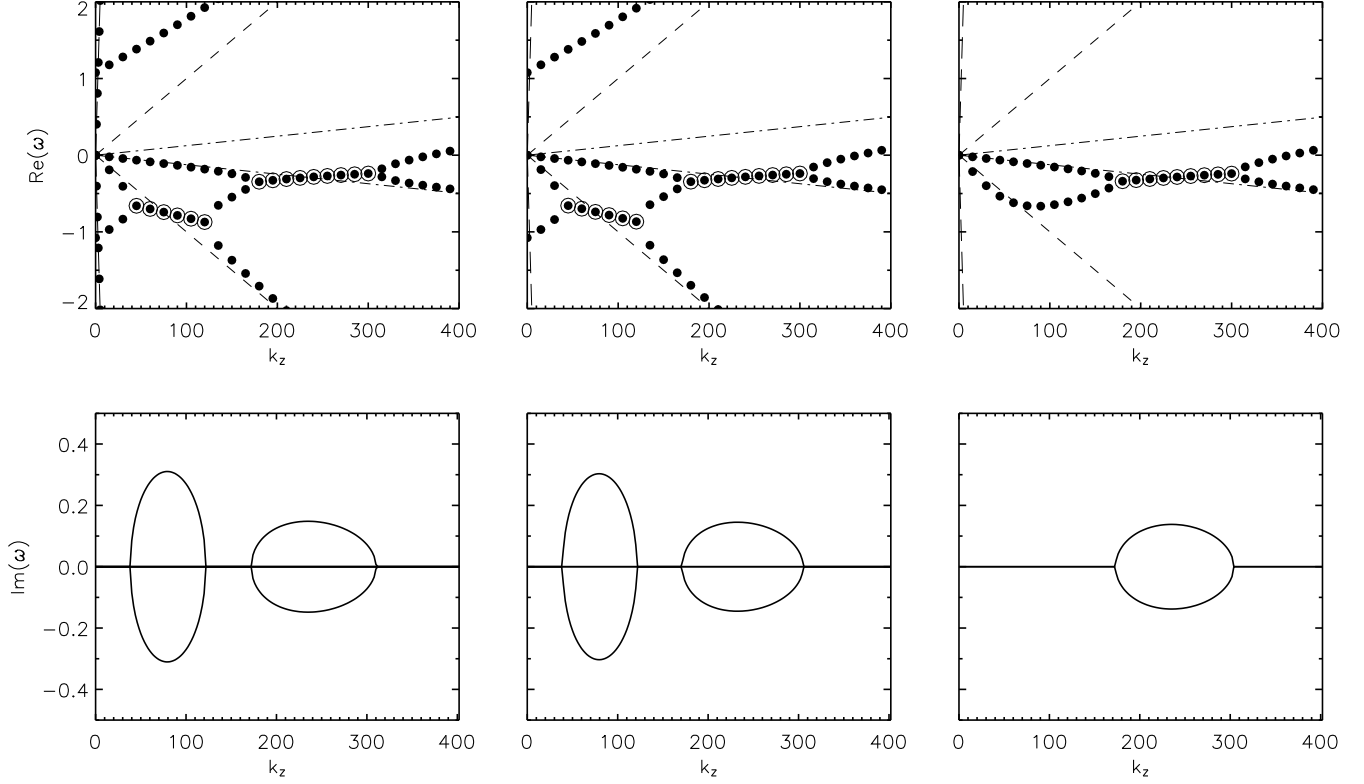


FIG. 4.— *Left panels:* Solutions to the full dispersion relation (25). *Central panels:* Solutions to the 4<sup>th</sup> order, approximate dispersion relation (41), with  $\epsilon_2 = \epsilon_3 = \epsilon_4 = 1$ . *Right panels:* Solutions to the 2<sup>nd</sup> order, approximate dispersion relation (44), with  $\epsilon_2 = \epsilon_3 = 1$  and  $\epsilon_4 = 0$ . All solutions correspond to a Keplerian disk with  $c_s = 0.05$ ,  $v_{Az} = 0.01$ , and  $v_{A\phi} = 0.40$ . Open circles in upper panels indicate unstable modes. Note that the phase velocities of the two instabilities (seen in either the leftmost or central upper panels and corresponding to Region II and III in §4.1) are similar to the phase velocities, positive and negative respectively, of the slow mode (point-dashed line) in the limit of no rotation. The fast magnetosonic modes can barely be seen close to the left axis in the upper left panel.

We now have all the elements to write equations (17) and (18) in terms of  $\delta B_r$  and  $\delta B_\phi$ . Using equations (36)-(38), valid in the limit  $\omega^2 \ll k_z^2 c_s^2$ , we obtain, in terms of the dimensionless variables,

$$\begin{aligned}
 -\omega^2 \delta B_r + 2i\omega \left[ 1 + \left( \frac{v_{A\phi}}{c_s} \right)^2 \right] \delta B_\phi = & - \left[ 2 \frac{d \ln \Omega}{d \ln r} + (k_z v_{Az})^2 - 2\epsilon_4 \frac{\omega}{k_z} \frac{v_{A\phi}}{v_{Az}} \right] \delta B_r \\
 & - ik_z v_{A\phi} v_{Az} \left[ 2\epsilon_1 + \epsilon_2 \left( \frac{v_{A\phi}}{c_s} \right)^2 \right] \delta B_\phi, \quad (39)
 \end{aligned}$$

$$\begin{aligned}
 -\omega^2 \delta B_\phi \left[ 1 + \left( \frac{v_{A\phi}}{c_s} \right)^2 \right] - i\omega \left[ 2 + \epsilon_4 \frac{\omega}{k_z} \frac{v_{A\phi}}{v_{Az}} \right] \delta B_r = & -(k_z v_{Az})^2 \delta B_\phi + ik_z v_{A\phi} v_{Az} \epsilon_3 \delta B_r. \quad (40)
 \end{aligned}$$

These equations are the generalization of the set of equations used to illustrate the physics behind the weak-field MRI as a system of masses coupled by a spring in a differentially rotating background. Indeed, in the incompressible limit and neglecting the curvature terms proportional to  $\epsilon_i$ , for  $i = 1, 2, 3, 4$ , we recover the set of equations presented elsewhere (Balbus & Hawley 1992, 1998).

Setting the determinant of the linear system (39)-(40) equal to zero and taking the limit  $v_{A\phi} \gg c_s$  provides the following approximate dispersion relation that is valid for strong toroidal fields<sup>6</sup>,

$$\omega^4 - (\kappa^2 + k_z^2 v_{Az}^2 + \epsilon_2 \epsilon_4 v_{A\phi}^2) \omega^2 - 2k_z v_{A\phi} v_{Az} (\epsilon_2 + \epsilon_3) \omega + k_z^2 v_{Az}^2 \left[ \frac{c_s^2}{v_{A\phi}^2} \left( k_z^2 v_{Az}^2 + 2 \frac{d \ln \Omega}{d \ln r} \right) - \epsilon_2 \epsilon_3 v_{A\phi}^2 \right] = 0. \quad (41)$$

Note that we have not neglected the factor  $c_s^2/v_{A\phi}^2$  in the last term in equation (41) because its contribution is non-negligible at large wavenumbers. The solutions to the dispersion relation (41), for a Keplerian disk with  $c_s = 0.05$ ,  $v_{Az} = 0.01$ , and

<sup>6</sup> Note that, had we taken the opposite limit, i.e.,  $c_s \gg v_{A\phi}$ , we would have recovered the dispersion relation (28) in the limit  $k_r/k_z \rightarrow 0$ .

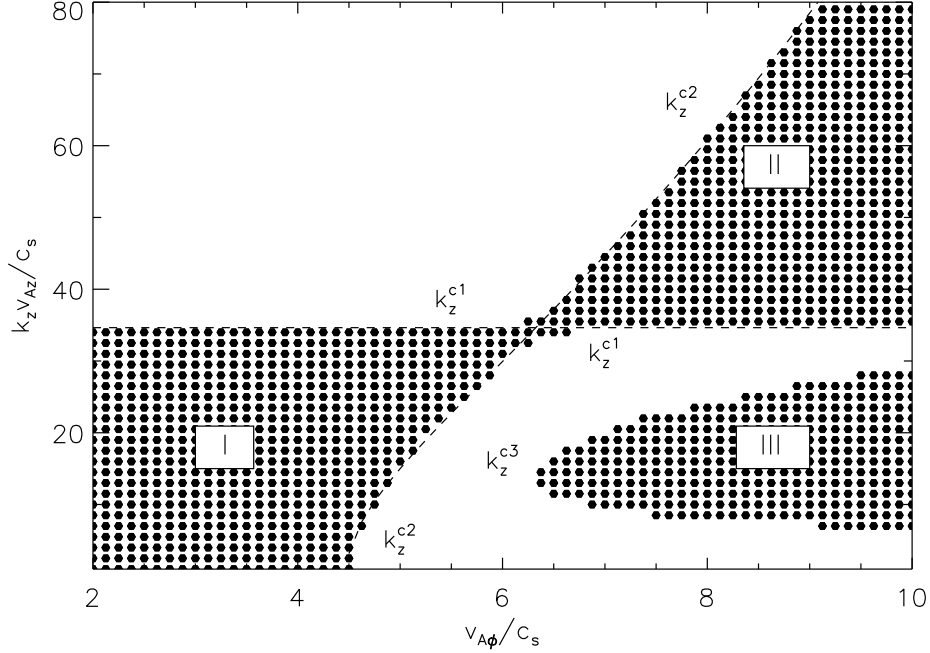


FIG. 5.— The black dots represent unstable modes satisfying the approximate instability criteria (43), described in §4.2. The dashed lines, labeled by  $k_z^{c1}$  and  $k_z^{c2}$ , are the limits of Regions I and II obtained analytically, also in §4.2. The onset of instability III is labeled by  $k_z^{c3}$ . As in Figure 3, we have assumed a Keplerian disk with  $c_s = 0.05$  and  $v_{Az} = 0.01$ .

$v_{A\phi} = 0.4$ , are shown in the central panels in Figure 4. For the sake of comparison, the left panels in the same figure show the solutions of the full dispersion relation (25). The solutions to the approximate dispersion relation (41) are in excellent agreement with the solutions to the general dispersion relation (25) for which  $\omega^2 \ll k_z^2 c_s^2$ .

Note that the term proportional to  $\epsilon_1$  is not present in equation (41). This feature has important consequences for us to understand the physics behind the stability of strongly magnetized compressible flows. It has been suggested (Curry & Pudritz 1995) that the magnetic tension term  $B_\phi \delta B_\phi / r_0$  (i.e., the one proportional to  $\epsilon_1$  in eq. [17]) is responsible for the stabilization of long-wavelength perturbations via the restoring forces provided by strong toroidal field lines in incompressible MHD flows. This argument sounds compelling, but we can see from the last term in equation (39) that the term proportional to  $\epsilon_1$  is not dynamically important for compressible flows in which  $v_{A\phi} \gg c_s$ . At least in the radial direction, it is rather the term proportional to  $\epsilon_2$  the one governing the deviation compared to the stability properties of weak toroidal fields. This is in complete agreement with equation (38).

The dispersion relation (41) is of the form

$$\omega^4 + b_2 \omega^2 + b_1 \omega + b_0 = 0. \quad (42)$$

For this 4<sup>th</sup> order equation to have complex roots (corresponding to unstable modes), its discriminant has to be negative, i.e.,

$$D_4(v_{A\phi}, k_z v_{Az}) = -4b_2^3 b_1^2 - 27b_1^4 + 16b_0 b_2^4 - 128b_2 b_0^2 + 144b_2 b_1^2 b_0 + 256b_0^3 < 0. \quad (43)$$

The modes satisfying this condition are shown as black dots in Figure 5. This analytical criterion agrees well with the numerical results for most of the parameter space ( $v_{A\phi}/c_s$ ,  $k_z v_{Az}/c_s$ ) with the exception of some of the unstable modes close to the separatrix of the Regions I and II, defined in §4.1.

*Limiting wavenumbers for Regions I and II.*— The modes satisfying the condition  $D_4 = 0$  correspond to the limits of Regions I, II, and III in Figure 5. Their analytical expressions, however, are complicated. Yet, some more progress can be made by realizing that the solutions to the second order equation obtained by simply dropping the  $\omega^4$  term in equation (41),

$$(\kappa^2 + k_z^2 v_{Az}^2 + \epsilon_2 \epsilon_4 v_{A\phi}^2) \omega^2 + 2k_z v_{A\phi} v_{Az} (\epsilon_2 + \epsilon_3) \omega - k_z^2 v_{Az}^2 \left[ \frac{c_s^2}{v_{A\phi}^2} \left( k_z^2 v_{Az}^2 + 2 \frac{d \ln \Omega}{d \ln r} \right) - \epsilon_2 \epsilon_3 v_{A\phi}^2 \right] = 0, \quad (44)$$

constitute a very good approximation to the solutions of the dispersion relation (25) whenever the frequencies of the modes satisfy  $\omega^2 \ll 1$ . This can be appreciated by comparing the left and right panels in Figure 4. The physics behind this approximation is not as direct as the physics behind the condition  $\omega^2 \ll k_z^2 c_s^2$ , but it can also be understood in terms of force balance, this time in the radial direction. The dispersion relation (44) can be obtained by neglecting the term proportional to  $\omega^2$  in equation (39),

setting to zero the determinant of the resulting linear system given by equations (39)-(40) and taking the limit  $v_{A\phi} \gg c_s$ . This approximation is equivalent to neglecting the term proportional to  $\omega$  in equation (17) and hence related to neglecting the radial acceleration experienced by a displaced fluid element.

Setting the discriminant of equation (44) to zero, gives an equation in  $k_z$  with solutions that are the limiting wavenumbers for the onset of instabilities I and II in Figure 5, i.e.,

$$D_2(v_{A\phi}, k_z v_{Az}) = (k_z v_{Az})^4 + \left[ \kappa^2 + 2 \frac{d \ln \Omega}{d \ln r} - v_{A\phi}^2 \left( \frac{v_{A\phi}^2}{c_s^2} - \epsilon_4 \frac{c_s^2}{v_{A\phi}^2} \right) \right] (k_z v_{Az})^2 + 2 \frac{d \ln \Omega}{d \ln r} \left[ \kappa^2 - v_{A\phi}^2 \left( \frac{v_{A\phi}^2}{c_s^2} - \epsilon_4 \frac{c_s^2}{v_{A\phi}^2} \right) \right] - \epsilon_4 v_{A\phi}^4 = 0. \quad (45)$$

Here, we have set  $\epsilon_2 = \epsilon_3 = 1$  but have explicitly left  $\epsilon_4$  to show that its contribution to the onset of instabilities I and II is not important when  $v_{A\phi} \gg c_s$ , as long as we are considering a rotationally supported disk. We mention, however, that the numerical solutions show that the contribution of the term proportional to  $\epsilon_4$  is small but not negligible for the unstable modes in region III. Neglecting the terms proportional to  $\epsilon_4$ , the solutions to equation (45) are simply

$$(k_z^c v_{Az})^2 = \frac{1}{2} \left[ \frac{v_{A\phi}^4}{c_s^2} - \left( \kappa^2 + 2 \frac{d \ln \Omega}{d \ln r} \right) \right] \pm \frac{1}{2} \left| \frac{v_{A\phi}^4}{c_s^2} - 4 \right|. \quad (46)$$

One of these solutions coincides always with  $k_{BH}$  (eq. [27]),

$$(k_z^{c1} v_{Az})^2 = -2 \frac{d \ln \Omega}{d \ln r}, \quad (47)$$

and the other one is

$$(k_z^{c2} v_{Az})^2 = \frac{v_{A\phi}^4}{c_s^2} - \kappa^2. \quad (48)$$

The modes with wavenumbers in the range  $[\min(k_z^{c1}, k_z^{c2}), \max(k_z^{c1}, k_z^{c2})]$  are unstable. In Figure 5, the critical curves  $k_z^{c1}(v_{A\phi})$  and  $k_z^{c2}(v_{A\phi})$  are shown, with the proper normalization, as dashed lines. The critical wavenumber  $k_z^{c2}$  in equation (48) will be positive only for toroidal Alfvén speeds larger than

$$v_{A\phi}^I = \sqrt{\kappa c_s}. \quad (49)$$

This is the critical value of the Alfvén speed beyond which the modes with longest wavelength in Region I (see Fig. 5) begin to be stable. For a Keplerian disk, the epicyclic frequency coincides with the orbital frequency and thus, in dimensionless units,  $\kappa^2 = 1$ . In this case, the critical Alfvén speed for  $k_z^{c2}$  to be positive corresponds to  $v_{A\phi} = 0.223$ . This is the reason for which the long-wavelength modes are already stable in the second plot in the left panel in Figure 1, where  $v_{A\phi} = 0.25$ .

Incidentally, we find that the values of toroidal Alfvén speeds for which the standard MRI gives the appropriate range of unstable modes are not as restricted to  $v_{A\phi} \ll c_s$  but rather to  $v_{A\phi} \ll \sqrt{\kappa c_s}$ . For  $v_{A\phi} \gtrsim \sqrt{\kappa c_s}$ , the standard MRI is stabilized at low wavenumbers. We point out that, Papaloizou & Szuszkiewicz (1992) found, by means of a global stability analysis of a compressible flow, that for a slim disk threaded only by a vertical field, the flow is stable if the vertical Alfvén speed exceeds, within a factor of order unity, the geometrical mean of the sound speed and the rotational speed. In dimensionless units, this stability criterion translates into  $v_{Az} \gtrsim \sqrt{c_s}$ .

The limiting case in which  $k_z^{c1} = k_z^{c2}$ , is reached for

$$v_{A\phi}^{II} = \sqrt{2 c_s}. \quad (50)$$

Note that, for  $c_s = 0.05$ , this corresponds to a value for the critical toroidal Alfvén speed of  $v_{A\phi} = 0.316$ . This situation is to be compared with the mode structure in the third plot in the left panel in Figure 1, where  $v_{A\phi} = 0.32$ .

*Limiting wavenumbers for Region III.*— In the previous section we presented some useful analytical approximations to describe the dependence of the critical values of the toroidal Alfvén speeds and wavenumbers defining Regions I and II on the different quantities characterizing the MHD flow. We could not, however, find simple analytical expressions to describe satisfactorily the corresponding behavior of the critical values defining Region III. We will describe next how the different unstable regions in Figure 3 depend on the magnitude of the sound speed and the steepness of the rotation profile.

## 5. DISCUSSION

In this section, we address several issues related to the importance of the curvature terms in determining the stability criteria obeyed by the solutions to the dispersion relation (25). We comment on some controversies raised by previous investigations that have treated the standard MRI taking into account, in various ways, either compressibility or curvature of the background magnetic field. We also comment on the importance in the outcome of the instabilities played by the magnetic tension produced by toroidal field lines in the limit of cold MHD flows. We highlight the similarities and differences of our findings with the results of Curry & Pudritz (1995), who also found the emergence of a new (but different) instability for strong toroidal fields in the case of an incompressible MHD flow. Finally, we address the potential implications of our findings for shearing box models in which magnetic tension terms, induced by the curvature of the background field, are not considered.

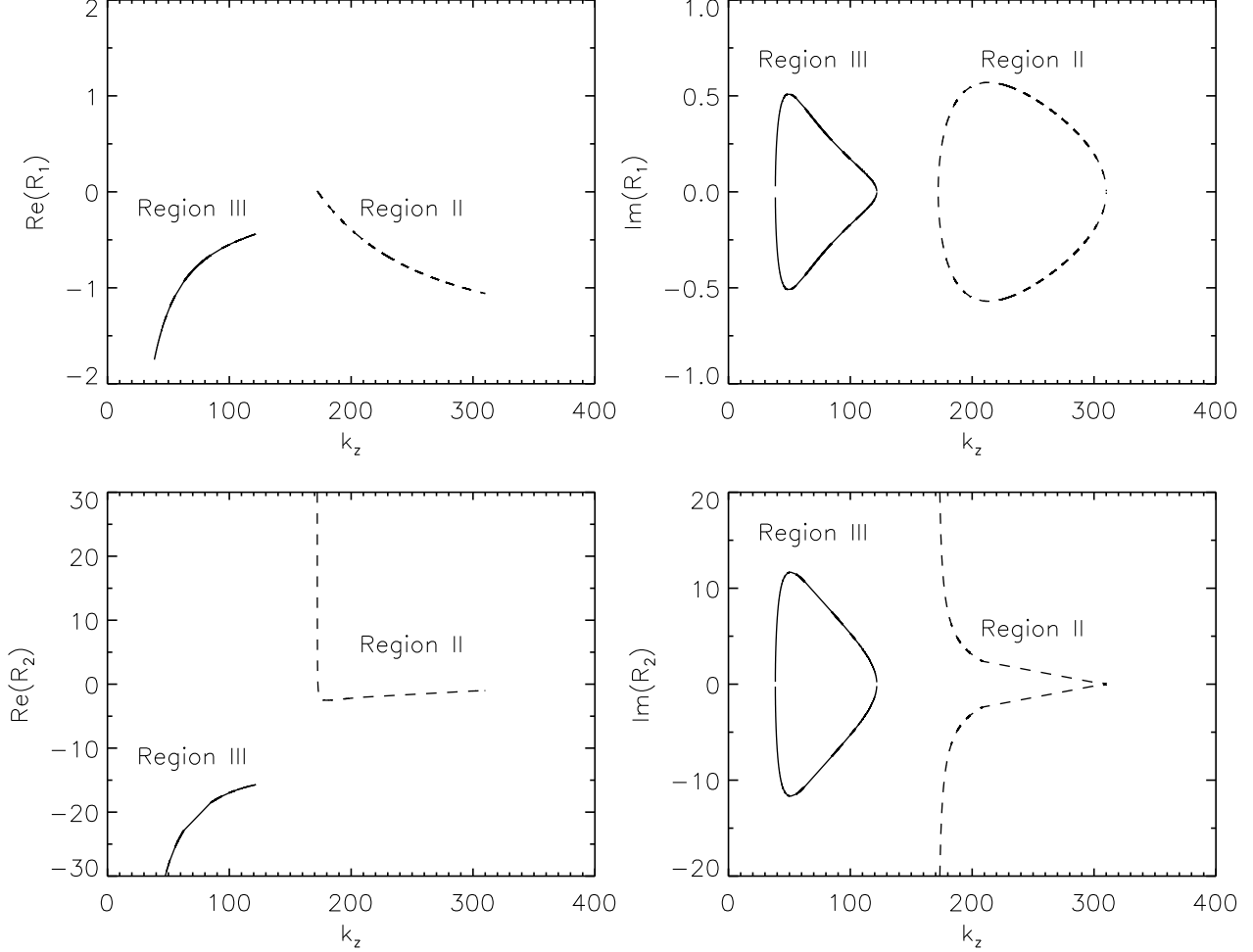


FIG. 6.— The importance of the curvature terms proportional to  $\epsilon_2$  and  $\epsilon_3$ , as defined by the ratios  $R_1$  (eq. [52]) and  $R_2$  (eq. [53]). For illustrative purposes, we have considered a Keplerian disk with  $c_s = 0.05$ ,  $v_{Az} = 0.01$ , and  $v_{A\phi} = 0.4$ .

### 5.1. Importance of Curvature Terms

In section §2 we mentioned that the terms proportional to  $\epsilon_i$ , for  $i = 1, 2, 3, 4$ , are usually neglected in local stability analyses due to their  $1/r_0$  dependence. Some of these terms, however, are also proportional to the magnitude of the toroidal field. In this paper, we found that, when strong toroidal fields are considered, these terms led to substantial modifications to the stability criteria of MHD modes known to be valid in the limit of weak fields. After solving the full problem, we are in a better position to understand why this is the case.

To illustrate the point, consider the ratio of the term proportional to  $k_z$  to the one proportional to  $\epsilon_2$  in equation (17) and the ratio of the term proportional to  $k_z$  to the one proportional to  $\epsilon_3$  in equation (18), i.e.,

$$R_1 \equiv \frac{\epsilon_2}{ik_z} \frac{v_{A\phi}^2}{v_{Az}} \frac{\delta\rho}{\delta v_{Ar}} \quad \text{and} \quad R_2 \equiv \frac{\epsilon_3}{ik_z} \frac{v_{A\phi}}{v_{Az}} \frac{\delta v_{Ar}}{\delta v_{A\phi}}. \quad (51)$$

In order to ensure that the contributions due to curvature are negligible in a local analysis regardless of the magnitude of the toroidal field component, we should be able to ensure that the conditions  $R_1 \ll 1$  and  $R_2 \ll 1$  hold in the limit of large  $k_z$  for any value of  $v_{A\phi} \lesssim 1$ . While it is encouraging that both dimensionless ratios are proportional to  $1/k_z$ , they are also proportional to the ratio of perturbed quantities, which we do not know *a priori*. It is only after having found the eigenfrequencies  $\omega(k_z)$  by taking into account all the curvature terms that we can properly address this issue.

We can calculate how the ratios  $R_1$  and  $R_2$  depend on the wavenumber  $k_z$  as follows. The ratio  $R_1$  can be recast using



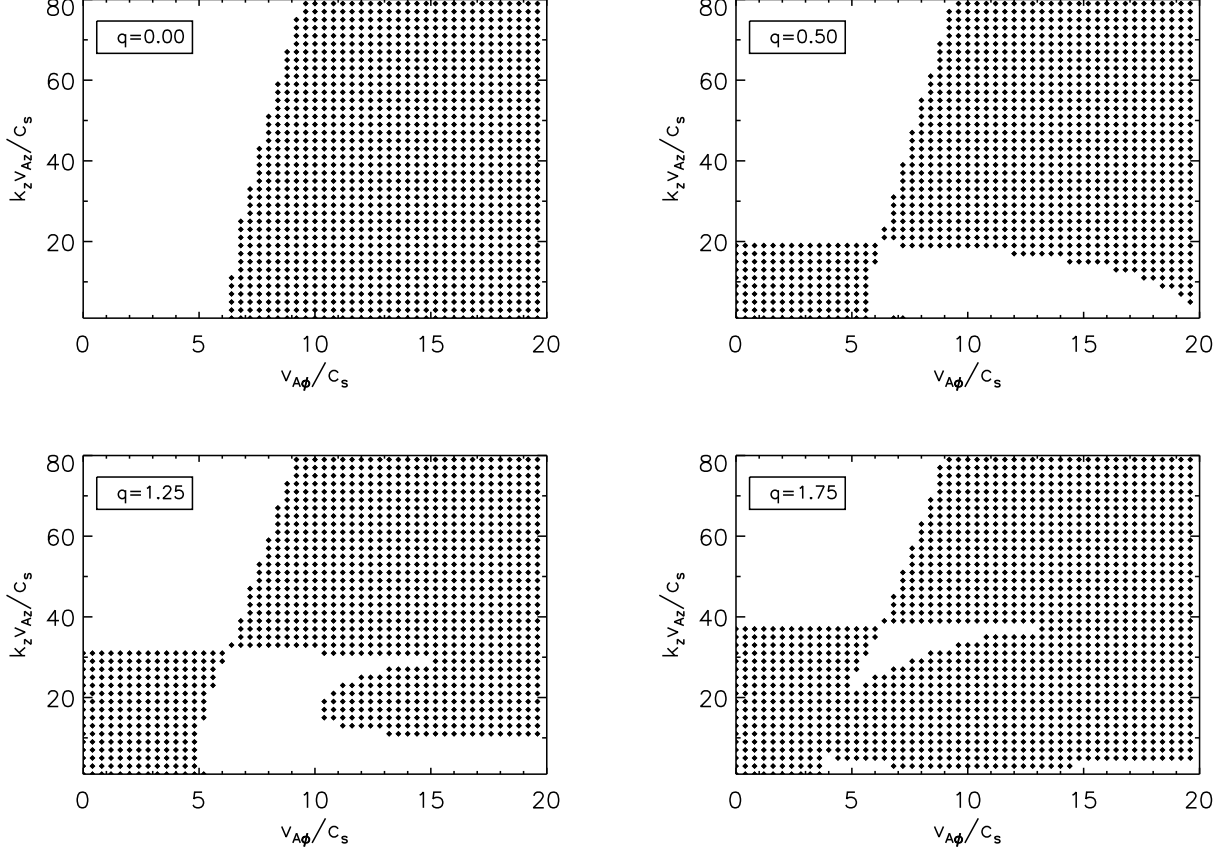


FIG. 7.— The black dots represent unstable modes obtained from solving numerically the dispersion relation (25) as a function of the toroidal Alfvén speed. As an example, we have assumed  $c_s = 0.05$  and  $v_{Az} = 0.01$ . In each plot, we consider different values of the rotational profile,  $q = -d \ln \Omega / d \ln r$ . Note that, the highest value of the local toroidal Alfvén speed considered here corresponds to the local circular velocity.

equations (38) and (39) as

$$R_1 = \frac{\epsilon_2}{k_z} \frac{v_{A\phi}}{v_{Az}} \left( \frac{v_{A\phi}}{c_s} \right)^2 \frac{\omega^2 - \left( 2 \frac{d \ln \Omega}{d \ln r} + k_z^2 v_{Az}^2 - 2 \epsilon_4 \frac{\omega}{k_z} \frac{v_{A\phi}}{v_{Az}} \right)}{2 \omega \left[ 1 + \left( \frac{v_{A\phi}}{c_s} \right)^2 \right] + k_z v_{Az} v_{A\phi} \left[ 2 \epsilon_1 + \epsilon_2 \left( \frac{v_{A\phi}}{c_s} \right)^2 \right]}. \quad (52)$$

In a similar way, we can rewrite the ratio  $R_2$  using equation (40) as

$$R_2 = \frac{\epsilon_3}{k_z} \frac{v_{A\phi}}{v_{Az}} \frac{\omega^2 \left[ 1 + \left( \frac{v_{A\phi}}{c_s} \right)^2 \right] - k_z^2 v_{Az}^2}{\omega \left[ 2 + \epsilon_4 \frac{\omega}{k_z} \frac{v_{A\phi}}{v_{Az}} \right] + \epsilon_3 k_z v_{Az} v_{A\phi}}. \quad (53)$$

For the sake of simplicity, let us consider a given value for the toroidal Alfvén speed, e.g.,  $v_{A\phi} = 0.4$ . Figure 6 shows the dependence of the ratios  $R_1$  and  $R_2$  on wavenumber for the unstable. The eigenfrequencies  $\omega(k_z)$  were obtained by solving equation (25) with  $\epsilon_i = 1$ , for  $i = 1, 2, 3, 4$ , considering a Keplerian disk with  $c_s = 0.05$  and  $v_{Az} = 0.01$ . The ratios  $R_1$  and  $R_2$  for the unstable modes (with  $v_{A\phi} = 8c_s$ ) in Regions II and III in Figure 3 are clearly identified. The complete mode structure corresponding to this case can be seen in the left panels of Figure 4.

It is important to stress that neither the real nor the imaginary parts of either  $R_1$  or  $R_2$  are negligible compared to unity even for Alfvén speeds of order a few times the sound speed. In fact, for the unstable modes, the ratio  $R_1$  is of order unity and the ratio  $R_2$  is in some cases larger than one by one order of magnitude. Their functional form is significantly different than the assumed  $1/k_z$ .

### 5.2. Magnetorotational Instabilities with Suprathermal Fields

In §3 we demonstrated that, when the toroidal magnetic field in a differentially rotating MHD flow becomes superthermal, three distinct instabilities can be identified, which we denote by roman numerals I, II, and III in Figure 3. We summarize the qualitative characteristics of these instabilities below.

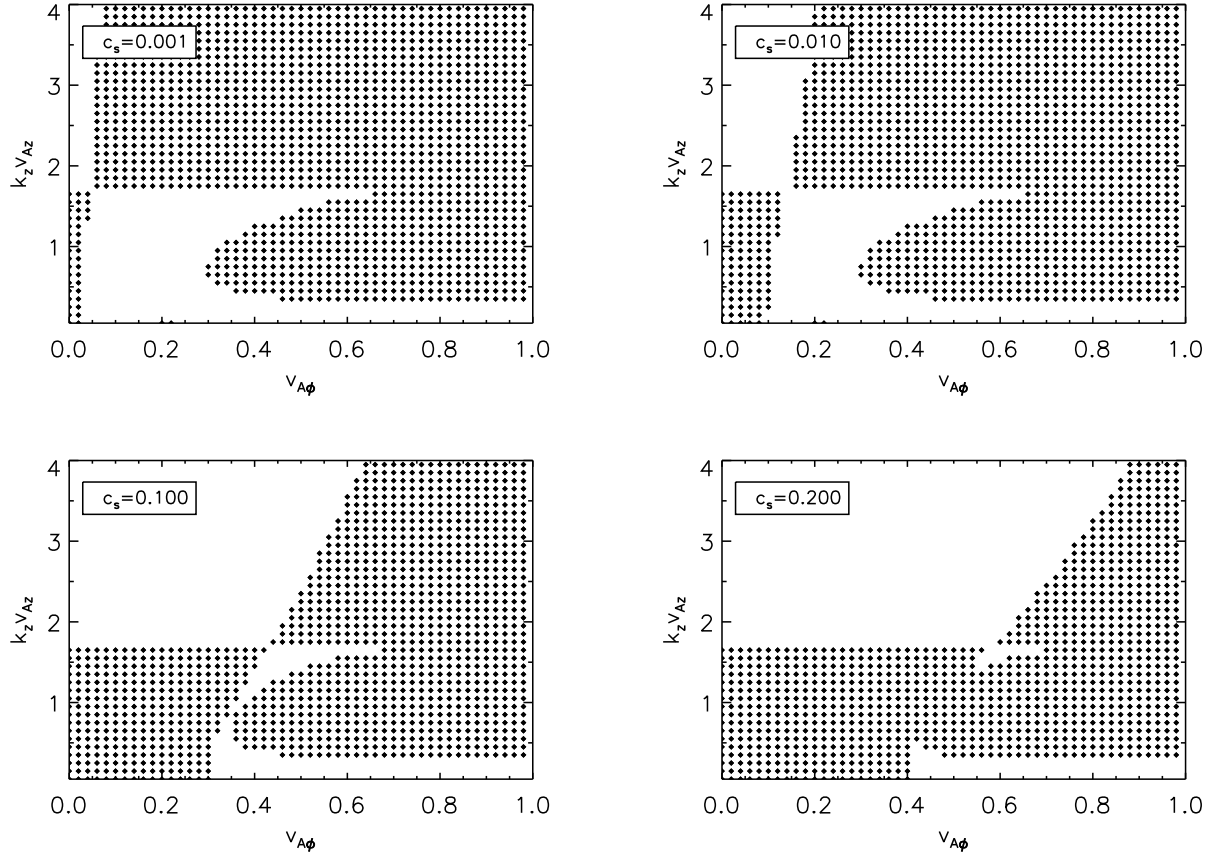


FIG. 8.— The black dots represent unstable modes obtained from solving the dispersion relation (25) numerically, for a Keplerian disk with  $v_{Az} = 0.01$ . In each plot, different values of the local sound speed,  $c_s$ , are considered. Note that in this case, the axes are not normalized by the particular value of the local sound speed, but rather by our initial choice of dimensionless variables, see §2.

In contrast to the weak-field MRI, all three instabilities correspond to compressible MHD modes. Moreover, while the traditional MRI corresponds to perturbations with negligible displacements along the vertical direction, this is not true for any of the three instabilities with superthermal toroidal fields. Instead, vertical displacements are an important characteristic of these instabilities and they occur with negligible acceleration, under a force balance between thermal and magnetic pressure. Finally, as in the case of the MRI, there is no significant acceleration along the radial direction but rather a force balance between magnetic tension, magnetic pressure, and thermal pressure.

In Figures 7 and 8 we study numerically the dependences of the three instabilities on the properties of the background flow. As also shown in the case of the weak-field MRI (Balbus & Hawley, 1991), instability I occurs only in differentially rotating flows, with radially decreasing angular velocity. However, instability I also requires the presence of a non-negligible thermal pressure. Either a radially increasing angular velocity or a superthermal toroidal field can suppress instability I and hence the traditional MRI.

Instability II is ubiquitous, whenever the background toroidal field of the flow is significantly superthermal. Indeed, it occurs even for flat (see Fig. 7) or very cold (see Fig. 8) flows. In a sense opposite to instability I, the steepness of the rotational profile determines the minimum unstable wavenumber, whereas the magnitude of the sound speed determines the minimum toroidal field strength required for the instability to occur. This instability seems to correspond to a generalization of the axisymmetric toroidal buoyancy (ATB) modes identified in Kim & Ostriker (2000), where the case  $c_s = 0$  was studied. In a similar way to instability II, the ATB modes with  $c_s = 0$  become unstable for all wavenumbers exceeding a critical value (for vertical modes this value is just given by  $k_{BH}$ ). When a finite sound speed is considered, however, thermal effects play an important role at small scales by completely stabilizing all the modes with wavenumbers larger than  $k_z^{c2}$  (eq. [48]).

Finally, instability III depends strongly on the rotational profile but very weakly on the sound speed. For rotationally supported flows (i.e., for  $v_{Aφ} \ll 1$ ), instability III occurs only for significantly steep rotational profiles, e.g.,  $q = |d \ln \Omega / d \ln r| \gtrsim 1.0$ , for the parameters depicted in Figure 7.

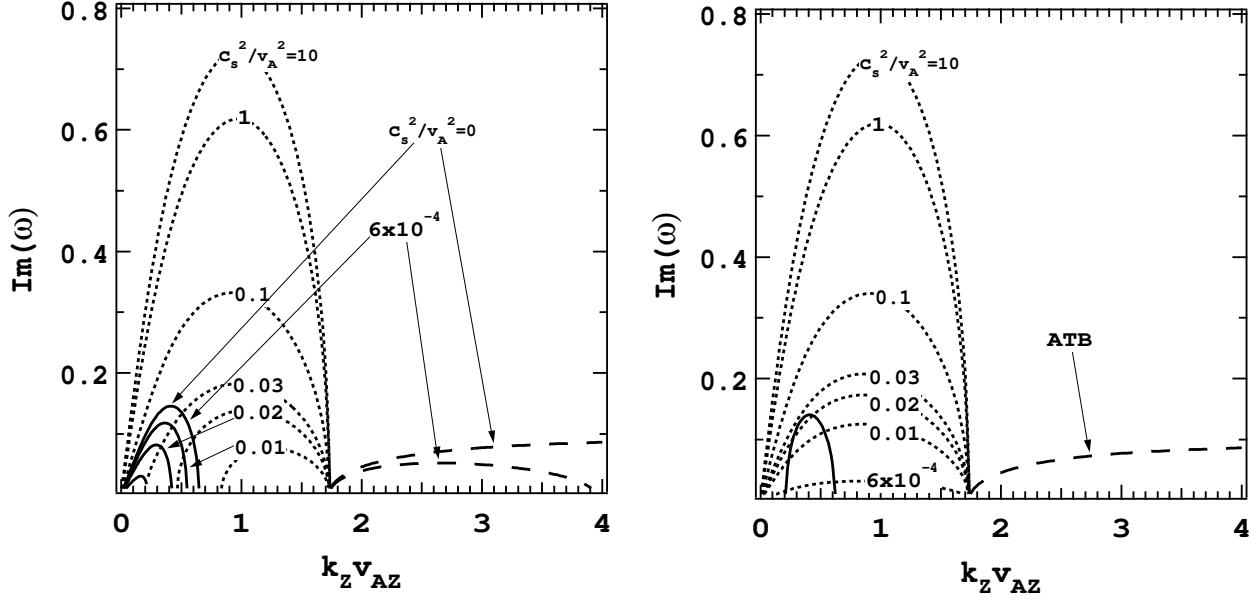


FIG. 9.— The growth rate evolution of the different instabilities defined in §4.1 for increasing magnetic field strength parameterized in terms of the ratio  $c_s^2/v_A^2$  for a fixed pitch angle  $i \equiv \tan^{-1}(v_{Az}/v_{A\phi}) = 25^\circ$ . *Left panels:* Growth rates of the unstable solutions to the full dispersion relation (25), when all curvature terms are taken into account. *Right panels:* Growth rates of the unstable solutions to the dispersion relation (30), i.e., when all curvature terms are neglected. In both cases, we have considered a vanishing ratio  $k_r/k_z$ ,  $v_{Az} = 0.05$ , and a Keplerian disk. The dotted lines, in both panels, show the stabilization of the standard MRI as the magnetic field becomes superthermal (instability I). The solid and dashed lines on the left panel show the growth rates corresponding to instability III and II respectively. As discussed in §3, these instabilities do not have a counterpart when the magnetic tension induced by bending of toroidal field lines is neglected. For completeness we have included, in the right panel, with solid and dashed lines the unstable solutions to equation (44) in Kim & Ostriker (2000). Instability II corresponds to a generalization of the ATB mode when thermal effects are accounted for.

### 5.3. Comparison to Previous Analytical Studies

Soon after the original paper by Balbus & Hawley (1991), Knobloch (1992) critiqued their approach to the study of local instabilities for lacking the contributions of curvature terms. Knobloch (1992) formulated the stability analysis of a vertically unstratified, incompressible disk as an eigenvalue problem in the radial coordinate. He found that the presence of a toroidal field component changes the conditions for the presence of the instability as well as the character of the unstable modes from purely exponentials to overstable (i.e.,  $\text{Re}[\omega] \neq 0$ ). Gammie & Balbus (1994) argued against Knobloch's findings regarding overstability, stating that it arose as a consequence of having kept only small order terms (like  $v_A/c_s$  and  $v_A/\Omega_0 r_0$ ). They concluded that these contributions would have been negligible had the flow been considered compressible.

As we comment in §4.2, Knobloch's dispersion relation is correct even in the limit  $c_s \gg v_{A\phi}$  (i.e., without the necessity of imposing strict incompressibility). Formally speaking, the linear term in  $\omega$  in equation (28) does break the symmetry of the problem allowing for unstable modes with  $\text{Re}(\omega) \neq 0$ . But it is also the case that, in the limit  $c_s \gg v_{A\phi}$ , because of the relative magnitude of the coefficients in the dispersion relation (28), we do not expect the stability properties of the flow to differ greatly from those described by the incompressible MRI. As we mention in §2.3, in order to see significant differences, the Alfvén speed would have to be of the order of the circular speed and therefore we do not expect the curvature terms to play a significant role on the stability of incompressible, rotationally supported flows. On the other hand, if we allow the MHD fluid to be compressible and consider the curvature of the background flow, the mode structure can be radically different from what is expected for the compressible MRI (c.f. Blaes & Balbus 1994). This is the case, even if the toroidal Alfvén speed exceeds the sound speed by a factor of a few without the necessity of violating the condition of a rotationally supported disk (see Fig. 1).

The stability of axisymmetric perturbations in weakly ionized and weakly magnetized shear flows was considered by Blaes & Balbus (1994). They showed that, when ionization equilibrium is considered in the two-fluid approach, strong toroidal fields can fully stabilize the flow. As part of their study, they relaxed the Boussinesq approximation in the case of a single fluid and argued that, to all orders in the field strength, the magnitude of  $B_\phi$  does not affect the stability criterion. As noted by Curry & Pudritz (1995), this conclusion was reached because the terms proportional to  $B_\phi/r_0$  were not included in the local analysis.

The behavior of the MRI in cold MHD shearing flows, has been addressed by Kim & Ostriker (2000). When performing their local analysis, these authors obtained the compressible version of the standard dispersion relation for the MRI and studied its solutions for different values of the ratio  $c_s^2/v_A^2$ . Analyzing their dispersion relation (i.e., their equation [57] which is equivalent to equation [30] in this study), Kim & Ostriker (2000) concluded that, when the magnetic field is superthermal, the inclusion of a toroidal component suppresses the growth rate of the MRI. Moreover, they found that, for a Keplerian rotation law, no

axisymmetric MRI takes place in very cold MHD flows if  $i < 30^\circ$ , where  $i$  is the pitch angle of the local magnetic fields,  $i \equiv \tan^{-1}(v_{Az}/v_{A\phi})$ .

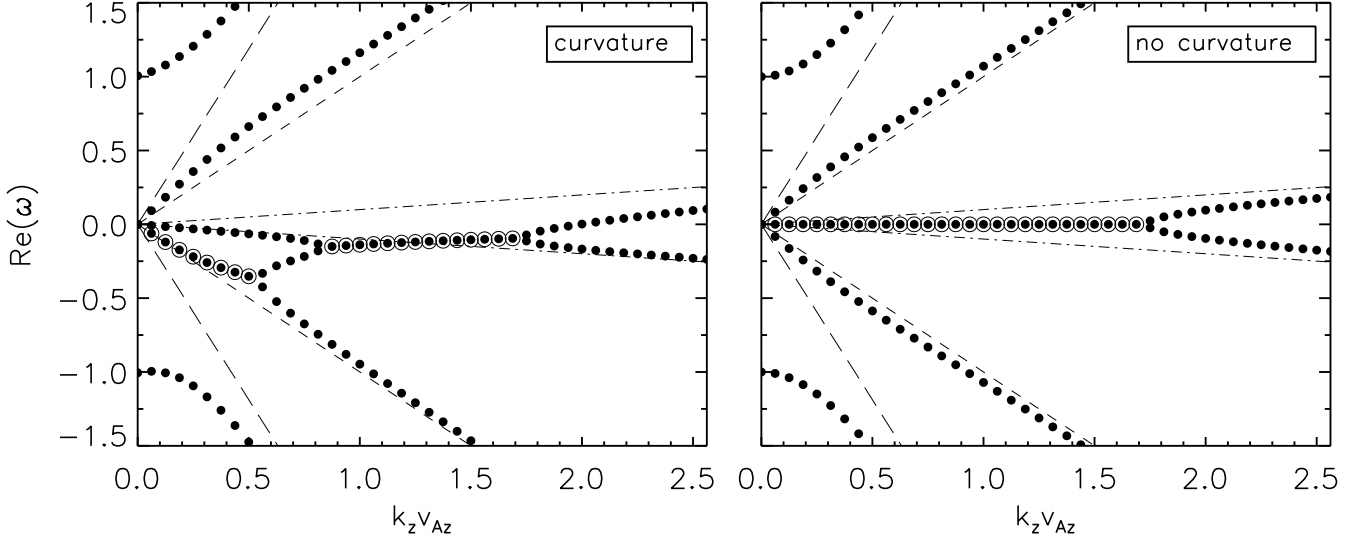


FIG. 10.— The real parts of the solutions to the dispersion relation (25) corresponding to  $c_s^2/v_A^2 = 0.01$  for a pitch angle  $i = \tan^{-1}(v_{Az}/v_{A\phi}) = 25^\circ$ , a vanishing ratio  $k_r/k_z$ ,  $v_{Az} = 0.05$ , and a Keplerian disk. *Left panel:* Solutions to the full dispersion relation (25), when all curvature terms are taken into account. *Right panel:* Solutions to the dispersion relation (26), i.e., when all curvature terms are neglected. Open circles indicate unstable modes. In both cases, the unstable modes with the shortest wavelength correspond to  $k_{BH}v_{Az}$ .

In §4 we showed that, depending on the strength of the toroidal field component, accounting for the finite curvature of the background magnetic field and the finite compressibility of the flow could be crucial in establishing which modes are subject to instabilities. In particular, we stated that both effects should be considered simultaneously whenever the local value of the toroidal Alfvén speed exceeds the geometric mean of the local sound speed and the local rotational speed (for a Keplerian disk). However, this analytic criterion was found to be relevant for the modes with frequencies satisfying the condition  $\omega^2 \ll k_z^2 c_s^2$ . Therefore, it is not obvious that we can trust this criterion in the limit  $c_s \rightarrow 0$ .

In order to see whether finite curvature effects do play a role in the stability of cold MHD flows we solved the complete dispersion relation (25) for a pitch angle  $i = 25^\circ$  and considered different values for the ratio  $c_s^2/v_A^2$ . Figure 9 shows the growth rates for the unstable modes of our dispersion relation (i.e., eq. [25]) and compares them to the ones of the dispersion relation obtained when the curvature terms are neglected (i.e., eq. [30]). In both cases, we have considered  $k_z \gg k_r$ ,  $v_{Az} = 0.05$ , and a Keplerian disk. The stabilization of the standard MRI (i.e., instability I) as the magnetic field becomes superthermal ( $v_A > c_s$ ) is evident (dotted lines in both panels). When the effects of magnetic tension are considered, not only does the growth rate of the MRI decrease faster for low values of  $c_s^2/v_A^2$  but the modes with longest wavelengths are no longer unstable (e.g. when  $c_s^2/v_A^2 = 0.01$ ). Because of this, the MRI is completely stabilized even for finite values of  $c_s^2/v_A^2$ . In contrast, when the curvature of the field lines is neglected, the growth rates decrease but the range of unstable modes remains unchanged as  $c_s \rightarrow 0$  (right panel in Figure 9); it is only when  $c_s = 0$  that the MRI is completely suppressed. For completeness, we present in Figure 10 the real parts of the solutions to the dispersion relation (25) for  $i = 25^\circ$ ,  $k_z \gg k_r$ ,  $v_{Az} = 0.05$ ,  $c_s^2/v_A^2 = 0.01$  and a Keplerian disk, in the cases where curvature terms are considered (left panel) and neglected (right panel). The stabilization of the MRI at low wavenumbers and the emergence of instability III are evident. Note that, from Figure 10, it is clear that the inclusion of magnetic tension terms can cause modifications to the mode structure when  $v_A \gg c_s$ , even when the toroidal and vertical components of the magnetic field are comparable.

In §5.2 we mentioned that instability II seems to be a generalization of the axisymmetric toroidal buoyancy (ATB) modes, identified by Kim & Ostriker (2000), that accounts for finite temperature effects. Further indication that this is indeed the case can be found in Figure 9 where we have plotted (dashed lines) the growth rates corresponding to instability II and the one corresponding to the ATB mode (solutions of equation [44] with  $\omega^2 \ll k_z^2 v_{Az}^2$  in Kim & Ostriker 2000). Although finite compressibility suppresses instability II at large wavenumbers, it is clear that, as  $c_s \rightarrow 0$ , the growth rates associated with instability II tend continuously to the growth rate of the cold ATB mode. For completeness, we have also included, in the right panel of Figure 9, the growth rate corresponding to the remaining unstable solution of equation (44) in Kim & Ostriker (2000) (solid line). This growth rate should be interpreted with great care since the aforementioned equation was derived under the condition  $\omega^2 \ll k_z^2 v_{Az}^2$ , which is not satisfied by the corresponding unstable mode. Nonetheless, we have included it to show the similarities that it shares with the growth rates corresponding to instability III (solid lines in the left panel) as  $c_s \rightarrow 0$ . Note that the growth rates corresponding to instability III increase as  $c_s \rightarrow 0$  and they saturate at  $c_s = 0$ . Although the higher critical wavenumber and the growth rate around this critical wavenumber seem to be the same for both instabilities, the differences between them at low wavenumbers is also evident. These differences become more dramatic as the pitch angle increases.

Curvature terms cannot, of course, be neglected in global treatments of magnetized accretion disks. It is, therefore, not surprising that new instabilities, distinct from the MRI, have already been found in global studies in which strong fields were considered. In particular, Curry & Pudritz (1995) performed a global stability analysis to linear axisymmetric perturbations of an incompressible, differentially rotating fluid, threaded by vertical and toroidal fields. They considered power-law radial profiles for the angular velocity and the toroidal and vertical components of the field. Each of these were parameterized as  $\Omega \propto r^{-a}$ ,  $B_\phi \propto r^{-b+1}$ , and  $B_z \propto r^{-c+1}$ , respectively. Most of their analysis dealt with a constant vertical field and they allowed variations of the exponents  $(a, b)$ , with the restriction that they correspond to a physical equilibrium state with a stationary pressure distribution. Although the majority of that paper dealt with global characteristics, they also performed a WKB analysis and concluded that, for  $3/2 \leq a = b \leq 2$  and  $v_{A\phi} < 1$ , the growth rate of unstable modes is suppressed on both short and long wavelengths and it approaches zero when  $v_{A\phi} \rightarrow 1$ . On the other hand, for  $a = b \neq 2$  and  $v_{A\phi} > 1$ , they found a new instability, with a growth rate that increased with  $v_{A\phi}$ . They call this the Large Field Instability (LFI) and showed that it can be stabilized for sufficiently large  $v_{Az}$ .

It is worth mentioning the major qualitative differences between the LFI and the new instability discussed in §3 that emerges for  $k_z < k_{\text{BH}}$  after the stabilization of the MRI. Although it is true that, for our instability to be present, it is necessary for the toroidal Alfvén speed to exceed the local sound speed, there is no need to invoke Alfvén speeds larger than the local rotational speed. This is in sharp contrast with the LFI which only appears for  $v_{A\phi} > 1$ . Regarding the range of unstable wavenumbers, the LFI remains unstable for  $k_z \rightarrow 0$ , albeit with diminishing growth rate for large values of  $v_{Az}$ . This is not the case for the new instability present at low wavenumbers in our study. This can be seen, for example, in the left panels in Figure 4. Perhaps the most noticeable difference is that the two instabilities in Curry & Pudritz (1995) that are present in the case  $a = b \neq 2$  do not seem to coexist under any particular circumstances. The instability present for  $v_{A\phi} < 1$  reaches zero growth for  $v_{A\phi} \rightarrow 1$ , while the LFI appears for  $v_{A\phi} = 1$  and its growth rate is proportional to  $v_{A\phi}$ . When compressibility is considered, however, the two new instabilities found in our study can coexist even for Alfvén speeds smaller than the local rotational speed.

#### 5.4. Implications for Shearing Box Simulations

In an attempt to capture the most relevant physics without all the complexities involved in global simulations, the shearing box approach has been widely used in numerical studies of magnetized accretion disks (see, e.g., Hawley, Gammie, & Balbus 1994). The aim of the shearing box approximation is to mimic a small region of a larger disk. The size of the box is usually  $H_z \times 2\pi H_z \times H_z$ , with  $H_z$  the thermal scale height of the isothermal disk. In this approach, it is common to adopt a pseudo-Cartesian local system centered at  $r_0$  and in corotation with the disk with an angular frequency  $\Omega_0$ , with coordinates  $x = r - r_0$ ,  $y = r_0(\phi - \Omega_0 t)$ , and  $z$ . The effects of differential rotation are then considered by imposing a velocity gradient in the radial direction. For a Keplerian accretion disk this is achieved by setting  $v_y = -(3/2)\Omega_0 x$ .

In most studies of unstratified shearing boxes, Alfvén speeds rarely exceed the value of the local sound speed (see, e.g., Hawley, Gammie, & Balbus 1995, 1996). This is mainly because they are designed to simulate the mid-plane of the disk where the flow is relatively dense. In §4.2, we have seen that, as long as the toroidal Alfvén speed does not exceed the critical value  $v_{A\phi}^2 = c_s \kappa$ , neglecting magnetic tension due to the curvature of toroidal field lines does not seem to affect the outcome of the MRI and hence the shearing box approach is well justified. However, when stratification is taken into account, usually by adopting a density profile of the form  $\rho \propto \exp[-z^2/(2H^2)]$  in the case of isothermal disks, the steep drop in the density beyond a few scale heights can potentially lead to a magnetically dominated flow, with Alfvén speeds larger than the critical value  $v_{A\phi}^2 = \kappa c_s$ .

As discussed in the introduction, Miller & Stone (2000) carried out three-dimensional MHD simulations to study the evolution of a vertically stratified, isothermal, compressible, magnetized shear flow. The simulations were local in the plane of the disk but vertically extended up to  $\pm 5$  thermal scale heights. This allowed them to follow the highly coupled dynamics of the weakly magnetized disk core and the rarefied magnetically-dominated (i.e.,  $\beta < 1$ ) corona that formed above the disk, for several (10 to 50) orbital periods.

Miller & Stone (2000) considered a variety of models, all sharing the same initial physical background, but different initial field configurations. In particular, they considered the following values:  $\Omega_0 = 10^{-3}$ ,  $2c_s^2 = 10^{-6}$  (so that  $H_z = \sqrt{2}c_s/\Omega_0 = 1$ ), and  $r_0 = 100$ . We mention some of the results they obtained for the models with initial toroidal fields (BY), which were qualitatively similar to the zero net  $z$ -field (ZNZ) models. After a few orbital periods, the presence of a highly magnetized (with plasma  $\beta \simeq 0.1 - 0.01$ ) and rarefied (with densities two orders of magnitude lower than the disk mid-plane density) corona above  $\sim 2$  scale heights is evident. Within both the disk and the corona, the “toroidal” component of the field ( $B_y$ ), favored by differential rotation, dominates the poloidal component of the field by more than one order of magnitude (with  $B_x^2 \simeq B_z^2$ ).

We can compare the predictions of our study to the mode structure that one might expect from the standard compressible MRI for the particular values of sound and Alfvén speeds found in the strongly magnetized corona by Miller & Stone (2000). To this end, we consider as typical (dimensionless) values  $c_s = 0.007$ ,  $v_{A\phi} = 0.1$  and  $v_{Az} = 0.01$ , where we have assumed  $\beta = 2(c_s/v_A)^2 \simeq 0.01$  and  $B_\phi = 10B_z$ . The largest features that their simulations are able to accommodate are those with  $k_z \sim 60$  (corresponding to a wavelength of 10 in the vertical direction). As it can be seen in Figure 11, the role of the curvature terms is not negligible in two different respects. First, it completely stabilizes the perturbations on the longest scales well inside the numerical domain. Second, the growth rate for the unstable modes is significantly reduced.

It is difficult to extrapolate from the present work to address how the instabilities discussed here would couple to buoyancy in the presence of a stratified medium like the one considered by Miller & Stone (2000). Shearing boxes might also suffer from other

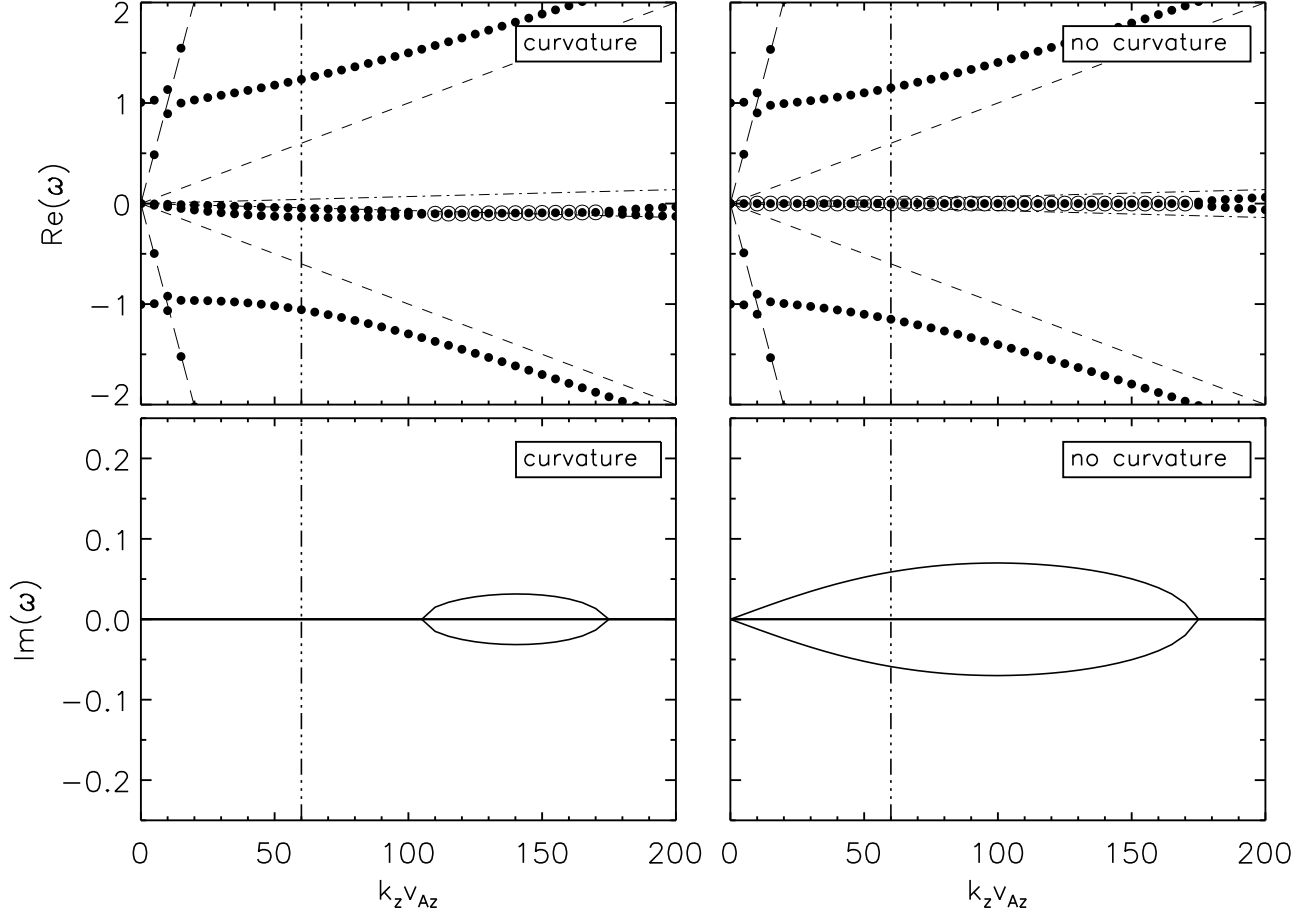


FIG. 11.— The implication of our study for shearing box simulations. *Left panels:* Solutions to the full dispersion relation (25), when all curvature terms are taken into account. *Right panels:* Solutions to the dispersion relation (26), i.e., when all curvature terms are neglected. In both cases, we have considered  $c_s = 0.007$ ,  $v_{Az} = 0.01$ ,  $v_{A\phi} = 0.1$ , and a Keplerian disk. Open circles in upper panels indicate unstable modes. The vertical line indicates the minimum wavenumber (i.e., largest wavelength) that can be accommodated in the simulations of a strongly-magnetized corona above a weakly magnetized disk by Miller & Stone (2000).

problems when used to model strongly magnetized plasmas (e.g., the shearing sheet boundary conditions in the radial direction might not be appropriate for strong fields). The question is raised, however, about whether, because of their own Cartesian nature, they constitute a good approach at all to simulating compressible flows in which superthermal toroidal fields are present. Despite the fact that the generation of strongly magnetized regions via the MRI in stratified disks seems hard to avoid, their stability properties will ultimately depend on both the use of proper boundary conditions and proper accounting of the field geometry.

## 6. SUMMARY AND CONCLUSIONS

In this paper we have addressed the role of toroidal fields on the stability of local axisymmetric perturbations in compressible, differentially rotating, MHD flows, when the geometrical curvature of the background is taken into account. In order to accomplish this task, without imposing restrictions on the strength of the background equilibrium field, we relaxed the Boussinesq approximation. In particular, we have studied under which circumstances the curvature terms, intimately linked to magnetic tension in cylindrical coordinate systems, cannot be neglected. We have shown that the MRI is stabilized and two distinct instabilities appear for strong toroidal fields. At least for large wavenumbers, the structure of the modes seems to be the result of a purely local effect that is accounted for when compressibility and curvature terms are consistently taken into account. In particular, we have demonstrated that, even for rotationally supported cylindrical flows, both curvature terms and flow compressibility have to be considered if, locally, the toroidal Alfvén speed exceeds the critical value given by  $v_{A\phi}^2 = (\kappa/\Omega)c_s\Omega r$  (in physical units).

There is little doubt that a realistic treatment of normal modes in magnetized accretion disks has to contemplate gradients in the flow variables over large scales and should, therefore, be global in nature. The results presented in this paper, however, provide the complete dispersion relation and, more importantly, analytic expressions for some of its solutions that should be recovered, in the appropriate limit, by a study of global modes in magnetized accretion disks, where compressibility effects are likely to be non negligible. We will address these issues in a future paper.

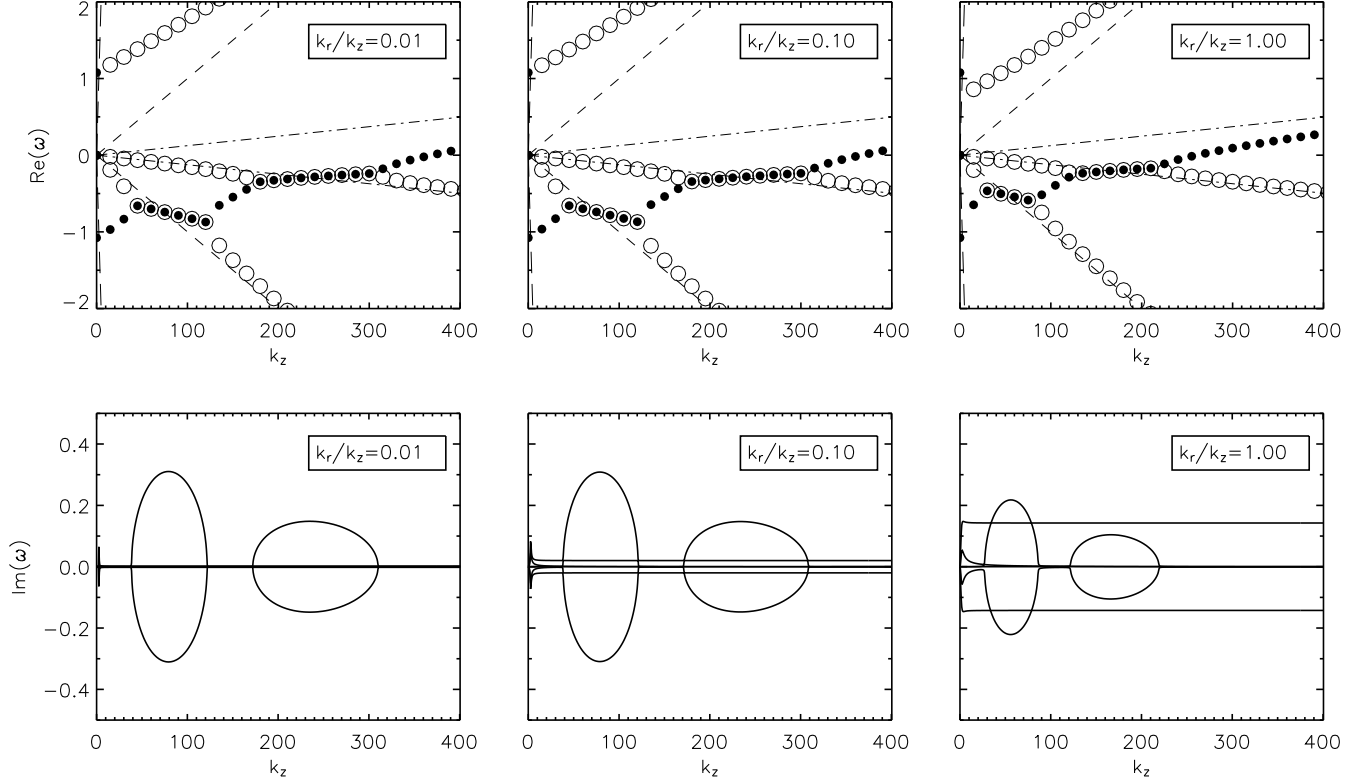


FIG. 12.— Solutions to the dispersion relation (25) for different values of the ratio  $k_r/k_z$ . The left, central, and right panels show the results for  $k_r/k_z = 0.01, 0.1, 1$  respectively. In all three cases, we have considered  $c_s = 0.05$ ,  $v_{Az} = 0.01$ ,  $v_{A\phi} = 0.4$ , and a Keplerian disk. Open circles in upper panels indicate unstable modes. The same instabilities that were present in the case with vanishing ratio  $k_r/k_z$  (left panels in Figure 4) can be clearly identified.

#### APPENDIX A

The central dispersion relation obtained in this study, i.e., equation (25), was derived considering axisymmetric perturbations in both the vertical and the radial directions. Throughout the majority of our analysis, however, we focused our attention on the modes with vanishingly small ratios  $k_r/k_z$ . Particular emphasis has been given to the study of these modes in the literature of weakly magnetized, differentially rotating disks, since these are the modes that exhibit the fastest growth rates (Balbus & Hawley 1992, 1998; Balbus 2003). After having analyzed the role played by magnetic tension forces due to the finite curvature of strong toroidal field lines on the stability of these modes, we are in a better position to understand their effects on the modes for which the ratio  $k_r/k_z$  is finite.

In Figure 12, we present the solutions to the dispersion relation (25) for three different ratios of the radial to the vertical wavenumber, i.e.,  $k_r/k_z = 0.01, 0.1, 1$ . For the sake of comparison, we have used in this figure the same parameters that we used in obtaining the left panels in Figure 4, for which the ratio  $k_r/k_z$  was considered to be vanishingly small; we have assumed  $c_s = 0.05$ ,  $v_{Az} = 0.01$ ,  $v_{A\phi} = 0.4$  and a Keplerian disk. In all the cases, the same instabilities (II and III) that were present in the case  $k_z \gg k_r$  can be clearly identified. Note however, that even for very small ratios  $k_r/k_z$  (e.g., left panels in Figure 12) some of the modes that were stable in the case  $k_z \gg k_r$  become unstable, albeit with negligible growth rate, when compared with the other unstable modes. It is also evident that in the limit  $k_z \gg k_r$ , the mode structure in Figure 12 tends continuously toward the mode structure in the left panels in Figure 4. It is this continuous behavior that ultimately justifies the study of modes with negligible ratio  $k_r/k_z$  in a local stability analysis.

In the case  $k_r = k_z$  (right panels in Figure 12), the value of the critical vertical wavenumbers for the onset of instabilities, i.e.,  $k_z^{c1}$  and  $k_z^{c2}$  in equations (47) and (48) respectively, are different with respect to the case in which  $k_z \gg k_r$  by a factor  $\sqrt{2}$ . This indicates that  $k_z$  and  $k_r$  play similar roles in establishing these critical wavenumbers. The growth rates of all these modes are reduced with respect to the case with  $k_z \gg k_r$ . This behavior is similar to the one observed in the case of weak magnetic fields. It is important to stress that, even for the modes with comparable values of vertical and radial wavenumbers, the general characteristics of the instabilities for strong toroidal fields that we discussed in §4.1 are insensitive to the inclusion of a non-negligible  $k_r$ .

The completely new feature in Figure 12 is the appearance of another instability with a growth rate that does not seem to depend on wavenumber; the terms proportional to  $ik_r$  in equation (25) are crucial for the appearance of this new instability. The mode that is unstable seems to correspond to the mode that becomes the Alfvén mode in the limit of no rotation. With

increasing values of the ratio  $k_r/k_z$ , the growth rates of the instabilities studied in §4.1 go to zero, but the new instability in Figure 12 persists. Note that for  $k_r \simeq k_z$  the growth rates of all the instabilities in Figure 12 are comparable.

As an aside, we point out that all the terms that are proportional to  $ik_r$ , as opposed to  $k_r^2$ , in equation (25) are also proportional to some factor  $\epsilon_i$  with  $i = 1, 2, 3, 4$ . All of these terms are negligible for sufficiently small ratios  $k_r/k_z$  no matter how strong the toroidal field is. Indeed, if we consider perturbations with small enough radial wavelengths, at some point, curvature effects will not be important. However, this is not true in the vertical direction. In that case, we can ignore the curvature terms only when the toroidal field is weak.

#### APPENDIX B

In the various sections of the present study, we have seen that the toroidal component of the magnetic field does play a role in determining the stability criteria. In fact, for superthermal fields and quasi toroidal configurations, it dictates the values of some of the critical wavenumbers for the onset of instabilities (see §4.2). A particular, simple case, in which the importance of considering both compressibility and magnetic tension terms can be appreciated, is the study of modes with negligible frequency, i.e., with  $\omega \ll 1$ . We can obtain the wavenumber of these modes by imposing  $\omega = 0$  to be a solution of the dispersion relation (25). We obtain, in physical dimensions,

$$(k_z^0)^2 = -2 \frac{d \ln \Omega}{d \ln r} \bigg|_0 \left( \frac{\Omega_0 r_0}{v_{Az}} \right)^2 + 2\epsilon_1 \epsilon_3 \left( \frac{v_{A\phi}}{v_{Az}} \right)^2 + \epsilon_2 \epsilon_3 \left( \frac{v_{A\phi}}{v_{Az}} \right)^2 \left( \frac{v_{A\phi}}{c_s} \right)^2. \quad (54)$$

In what follows, let us consider a rotationally supported disk whose rotational profile is not too steep (i.e.,  $|d \ln \Omega / d \ln r|$  is of order unity). The Alfvén speed  $v_{Az}$  appears in all three terms on the right hand side of equation (54) and therefore it does not play a role in determining the relative magnitudes between them. Unlike the second term, the third term is not necessarily small with respect to the first one, when superthermal fields are considered. In this case, it seems again (see §4.2) safe to neglect the curvature term proportional to  $\epsilon_1 \delta v_{A\phi}$  in equation (17). However, had we neglected the curvature term proportional to  $\epsilon_2 \delta \rho$  in equation (17) or the one proportional to  $\epsilon_3 \delta v_{Ar}$  in equation (18), we would have missed the important impact that the third term in equation (54) has on the stability of modes with  $\omega \rightarrow 0$ , in the limit of strong toroidal fields (see Fig. 3). This is somewhat counterintuitive because there does not seem to be any *a priori* indication about which of the magnetic tension terms (related to the curvature of the toroidal field component) is less relevant in the original set of equations (16)-(22) for the perturbations. This particular example illustrates the risks associated with neglecting terms that are not strictly 2<sup>nd</sup> order in the perturbed quantities but rather address the geometrical characteristics of the background in which the (local) analysis is being carried out.

From equation (54) it is also straightforward to see under which circumstances it is safe to neglect the curvature terms. For subthermal fields,  $k_z^0$  will not differ significantly from  $k_{BH}$  (eq. [27]) regardless of the geometry of the field configuration. This is because, if the field is weak enough ( $v_A \ll c_s$ ), no matter how strong of a (subthermal)  $B_\phi$  component we consider, the second and third term are negligible with respect to the first one. We conclude this short analysis by commenting that, while a strong vertical field plays a stabilizing role, in the sense that it drives  $k_z^0$  toward small values leaving all modes with shorter wavelengths stable, the consequences of considering strong toroidal fields is a little more subtle as it can be seen in the evolution of the structure of the modes in Figure 1.

We thank Eliot Quataert, Jim Stone, Charles Gammie, and Wolfgang Duschl for useful comments and discussion in different stages of this study. We thank an anonymous referee for pointing out the connection between instability II and the ATB modes. We are also grateful to Ethan Vishniac for encouraging us to address the limit discussed in Appendix A. We also thank the Institute for Advanced Study for their hospitality during part of this investigation. This work was partially supported by NASA grant NAG-513374

#### REFERENCES

- Balbus, S. A. 2003, *ARA & A*, 41, 555  
 Balbus, S. A., & Hawley, J. F. 1991, *ApJ*, 376, 214  
 ———. 1992, *ApJ*, 392, 662  
 ———. 1998, *Rev. Mod. Phys.*, 70, 1  
 ———. 2002, *ApJ*, 573, 749  
 Blaes, O. M., & Balbus, S. A. 1994, *ApJ*, 421, 163  
 Blaes, O. M., & Socrates, A. 2001, *ApJ*, 553, 987  
 Bourke, T. L., & Goodman, A. A. 2003, In *Star Formation at High Angular Resolution*, ASP Conf. Ser., Vol. S-221, eds. M. G. Burton, R. Jayawardhana, and T. L. Bourke (astro-ph/0401281)  
 Curry, C., & Pudritz, R. E. 1995, *ApJ*, 453, 697  
 Dubrulle, B., & Knobloch, E. 1993, *A&A*, 274, 667  
 Gammie, C. F., & Balbus, S. A. 1994, *MNRAS*, 270, 138  
 Hawley, J. F., Gammie, C. F., & Balbus, S. A. 1994, in *ASP Conf. Ser. 54, The First Stromlo Symposium: The Physics of Active Galaxies*, ed. G. V. Bicknell, M. A. Dopita, & P. J. Quinn (San Francisco:ASP), 53  
 ———. 1995, *ApJ*, 440, 742  
 ———. 1996, *ApJ*, 464, 690  
 Kim, W. T., & Ostriker, E. C. 2000, *ApJ*, 540, 372  
 Knobloch, E. 1992, *MNRAS*, 255, 25  
 Kudoh, T., Matsumoto, R., & Shibata, K. 2002, *PASJ*, 54, 121  
 Machida, M., Hayashi, M. R., & Matsumoto R. 2000, *ApJ*, 532, L67  
 Miller, K. A., & Stone, J. M. 2000, *ApJ*, 534, 398  
 Myers, P. C., & Goodman A. A. 1988, *ApJ*, 326, L27  
 Ostriker, E. C., Stone, J. M., & Gammie, C. F. 2001, *ApJ*, 577, 524  
 Pariev, V. I., Blackman, E. G., & Boldyrev, S. A. 2003, *A&A*, 407, 403  
 Papaloizou J., & Szuszkiewicz E. 1992, *Geophys. Astrophys. Fluid Dyn.*, 66, 223  
 Press, W. H., Flannery, B. P., Teukolsky, S. A., & Vetterling, W. T. 1992, *Numerical Recipes* (Cambridge: University Press)  
 Pringle, J. E. 1989, *MNRAS*, 236, 107  
 Quataert, E., Dorland, W., & Hammett, G. W. 2002, *ApJ*, 577, 524  
 Sano, T., & Miyama, S. M. 1999, *ApJ*, 515, 776